REPORT DOCUMENTATION PAGE

Form Approved
OMB No. 0704-0188

1. REPORT DATE *(DD-MM-YYYY)*	2. REPORT DATE	3. DATES COVERED *(From - To)*
10 February 2003	February 2003 FINAL TECH.	1/15/00 to 1/14/03

4. TITLE AND SUBTITLE

ULTRAWIDEBAND RADIO RANGING STUDIES

5a. CONTRACT NUMBER

5b. GRANT NUMBER

N00014-00-1-0221

5c. PROGRAM ELEMENT NUMBER

6. AUTHOR(S)

Dr. Robert A. Scholtz

5d. PROJECT NUMBER

5e. TASK NUMBER

5f. WORK UNIT NUMBER

7. PERFORMING ORGANIZATION NAME(S) AND ADDRESS(ES)

Department of Electrical Engineering
University of Southern CAlifornia
Los Angeles, CA 900890-2565

8. PERFORMING ORGANIZATION REPORT NUMBER

9. SPONSORING/MONITORING AGENCY NAME(S) AND ADDRESS(ES)

Office of Naval Research
Ballston Centre Tower One
800 North Quincy Street
Arlington, VA 22217-5660

10. SPONSOR/MONITOR'S ACRONYM(S)

ONR

11. SPONSORING/MONITORING AGENCY REPORT NUMBER

12. DISTRIBUTION AVAILABILITY STATEMENT

Unclassified - No limits

DISTRIBUTION STATEMENT A
Approved for Public Release
Distribution Unlimited

13. SUPPLEMENTARY NOTES

Abstract: The research grant supported the study of UWB radio ranging advantages and issues caused primarily by the wide radio frequency bandwidth and fine time resolution capabilities of these systems. Significant progress was made in understanding how to cooperatively range in a dense multipath environment. In addition, UWB propagation measurements were made in a shipboard environment to determine the difficulties in positioning using RF signals in a large metallic enclosure, and issues in sharing a large RF bandwidth with other narrowband radio systems were explored.

15. SUBJECT TERMS

Ultrawideband, propagation, antennas, radios

16. SECURITY CLASSIFICATION OF:			17. LIMITATION OF ABSTRACT	18. NUMBER OF PAGES	19a. NAME OF RESPONSIBLE PERSON
a. REPORT	b. ABSTRACT	c. THIS PAGE			Milly Montenegro
Final				5	19b. TELEPONE NUMBER *(Include area code)* (213) 740-7875

Standard Form 298 (Rev. 8-98)
Prescribed by ANSI-Std Z39-18

20030221 077

UWB Radio Ranging Studies

A Final Report to the Office of Naval Research
on Contract No. N00014-00-1-0221

R. A. Scholtz, Principal Investigator
University of Southern California
Los Angeles, CA 90089-2565
scholtz@usc.edu

Abstract: The research grant supported the study of UWB radio ranging advantages and issues caused primarily by the wide radio frequency bandwidth and fine time resolution capabilities of these systems. Significant progress was made in understanding how to cooperatively range in a dense multipath environment. In addition, UWB propagation measurements were made in a shipboard environment to determine the difficulties in positioning using RF signals in a large metallic enclosure, and issues in sharing a large RF bandwidth with other narrowband radio systems were explored.

Research Summary

The work associated with this contract has focused on the application of ultrawideband (UWB) radio to radio ranging systems. Three distinct research problems have been explored:

- The design of cooperative radio ranging algorithms,
- The evaluation of UWB radio interference to other receivers,
- The propagation of UWB signals in a shipboard environment.

Our research in these areas is documented in the following sections, with the names listed being the participating graduate students. Those items not completely described in this report are attached as appendices.

The design of UWB ranging algorithms (Joonyong Lee)
Since UWB ranging study was proposed to ONR, a signal processing technique for the detection of the earliest arriving signal (sometimes referred to as the direct path signal) has been developed as a key factor for accurate ranging. Our initial work was reported in (abstract only):

> **Joonyong Lee and R. A. Scholtz, "Time of Arrival Estimation of the Direct Path Signal in UWB Communications,"** ***National Radio Science Meeting (URSI)*****, Boulder CO, January 2001.**
>
> **Abstract**: The exceptionally fine time resolution and penetration capability of UWB signals enable potential applications involving high-resolution ranging systems. For this purpose, accurate detection of the time of arrival of the direct path signal is essential. Complex geometry and dynamics containing many unknown spatial variables are involved in UWB propagation. The direct path signal is not always the strongest in a

multipath environment, especially in beyond line of sight propagation. This makes ranging to the full capabilities of ultra-wideband signals challenging.

A signal processing technique for estimating the time of arrival of a direct path signal in the presence of dense multipath interference is introduced. The basic idea is to select a set of candidate propagation path delays for the received signal and determine the one that satisfies a certain decision criterion. The key parameters used in the decision criterion are the relative strength and the relative time displacement between the strongest path and a potential direct path signal. Thresholds are applied to these parameters based on the characteristics of the initial portion of the signal.

The analysis of different kinds of potential errors is presented. The two kinds of errors encountered in these systems are (1) an early false alarm error and (2) a missed direct path error. An early false alarm error occurs when a signal detection caused by noise and/or interference is declared prior to arrival of the direct-path signal. A missed direct path error occurs when a reflected signal path is declared to be the direct path. The probability of early false alarm error can be approximated by a simple exponential form using techniques employed in the evaluation of high level crossing probability for a continuous random process. Stochastic characterization of the initial signal structure is required to refine the decision criterion.

The research continued with an effort to optimize choice of threshold parameters used in the ranging algorithm. An error analysis was performed based on the statistical description of the initial signal structure. This statistical modeling was done with 527 indoor UWB pulse response measurements with blocked LoS(Line of Sight). The joint distribution of the relative strength and the relative time displacement between the strongest path and the first arriving path was modeled and independence between these two parameters was shown using X^2 test. Portions of this work were reported by

R. A. Scholtz, UWB Radio Ranging Studies, *Marine Corps Science and Technology Program Review*, 2 March 2001, at Quantico, VA.

The complete description of this work, including algorithm design, statistical modeling, parameter selection, propagation anomalies, and techniques for cooperative ranging were were documented in the following journal paper.

Joon-Yong Lee and Robert A. Scholtz, "Ranging in a Dense Multipath Environment Using an UWB Radio Link," *IEEE Journal on Selected Areas in Communications*, vol. 20, no. 12, pp. 1677-1683, December 2002.

ABSTRACT: A time-of-arrival (ToA)-based ranging scheme using an ultra-wideband (UWB) radio link is proposed. This ranging scheme implements a search algorithm for the detection of a direct path signal in the presence of dense multipath, utilizing generalized maximum-likelihood (GML) estimation. Models for critical parameters in the algorithm are based on statistical analysis of propagation data and the algorithm is tested on another independent set of propagation measurements. The proposed UWB ranging system uses a correlator and a parallel sampler with a high-speed measurement

capability in each transceiver to accomplish two-way ranging between them in the absence of a common clock.

A UWB range ambiguity function has been newly defined and its theory has been developed. It is different from the narrowband ambiguity function because it employs a time scaling factor rather than a Doppler shift parameter. This function serves to define the limits of time resolution for UWB matched filter receivers. This and issues of sampling methods were published in the following paper.

Joon-Yong Lee and Robert A. Scholtz, "Problems in Modeling Ultra-Wideband Channels," *Asilomar Conference on Signals, Systems, and Computers*, November 2002.

ABSTRACT: Ultrawideband (UWB) channel models pose a new set of problems to the designer. The very wide radio frequency bandwidth employed by a UWB radio means that more structure of the channel is exposed by the fine time resolution of the UWB radio receiver. Issues pertinent to the design and simulation of UWB communication and ranging systems will be illustrated through a set of UWB measurements.

Interference issues in the deployment of UWB Radios (Joonyong Lee and Robert Weaver)
The UltRa Lab carried out an effort to determine the capabilities of a UWB radio in the presence of interference and under a regulation that might be acceptable to the FCC. This involved most of the graduate students, including those supported by ONR. Here is the citation and abstract of an invited paper on the subject, which credits ONR support for part of the work.

R. A. Scholtz, R. Weaver, E. Homier, J. Lee, P. Hilmes, A. Taha, and R. Wilson, "UWB Radio Deployment Challenges," Personal Indoor Mobile Radio Conference 2000, London, September 2000.

ABSTRACT: The challenges related to the deployment of ultrawideband (UWB) radios are posed in terms of interference issues that UWB radio systems will encounter. The problem of coexistence with a Global Positioning System (GPS) receiver is used as an experimental example. Calculation of an upper bound to UWB transmitter power illustrates the effect of one possible type of regulation for a given UWB antenna system. The interference environment for a UWB receiver is used to lower bound the UWB transmitter power at a given data rate, and sample measurements are provided.

Later we were contacted by the American Radio Relay League and asked to evaluate the effect of interference from our equipment on one of their more sensitive analog radio receivers. This exercise turned out to be quite involved, the problems having to do with sensitivity, dynamic range, and nonlinearities in the front end of the victim receiver.

R. D. Wilson, R. D. Weaver, M.-H. Chung and R. A. Scholtz, "Ultra-Wideband Interference Effects on an Amateur Radio Receiver," *2002 IEEE Conference on Ultra Wideband Systems and Technologies, Baltimore MD, May 2002.*

ABSTRACT: This paper illustrates the complexity of issues that arise in the accurate measurement and interpretation of ultra-wideband (UWB) interference effects in narrowband receivers. The behavior of an amateur radio receiver in the presence of sinusoidal and UWB interference is studied. We characterize antenna response and receiver non-linearities, which lead to an understanding of UWB effects on the receiver output during outdoor response measurements as a function of range and antenna orientation.

Propagation in the shipboard environment (Joonyong Lee and Robert Weaver)
Much of the work that we are doing on UWB ranging algorithms is environment dependent. To explore an environment of interest to the Navy, we took propagation test equipment to the Naval Facilities Engineering Support Center at Port Hueneme, and performed propagation tests in the empty cargo hold of the *USS Curtiss*. Our contact there was

Steve Gunderson, (805) 982-1262, steve@nfesc.navy.mil

These tests indicated that pulse response functions in this environment can be 10 or more times longer than typical indoor measurements in an office building. This indicates that special care must be taken to avoid interpulse interference in UWB modulation and receiver design for shipboard systems. These measurements were also described at the above mentioned *Marine Corps Science and Technology Program Review*, 2 March 2001, at Quantico, VA.
The results of these tests were eventually reported in thefollowing:

Appendix A: USC UltRa Lab: Shipboard Environment Characterization, in Naval Total Asset Visibility (NTAV) Tests on the SS Curtiss, Port Hueneme, CA 25 September – 6 October 2000, Technical Report March 2002 (Appendix coauthored by S. Gunderson, R. Scholtz, K. Chugg, R. Weaver, J. Lee, C. Corrada, E. Homier, and R. Wilson).

Other related UWB radio talks (not mentioned above) presented by the investigator

- R. A. Scholtz, "Ultrawideband Communication Systems," ARO MURI Program in Chaotic Communications, Winter School 2000, University of California, San Diego,
- Jan. 23-26, 2000.
- `R. A. Scholtz, "`Multiple Access with Time-Hopping Impulse Modulation," Broadband Space-Time Seminar, Acorn Technologies, Inc., Pacific Palisades, February 11, 2000.
- R. A. Scholtz, "Ultrawideband Radio," Workshop on Ultrawideband Communications (sponsored by the Office of Naval Research), Berkeley Wireless Research Center, May 16, 2000.
- R. A. Scholtz, "Ultrawideband Radio," first speaker (invited) at the NSF Wireless Grantees Workshop, Washington DC, Feb. 20-21, 2001.
- R. A. Scholtz, "Ultrawideband Radio Ranging Studies," first academic speaker, Marine Corps Science and Technology Program Review, Quantico, VA March 2, 2001.
- R. A. Scholtz, Seminar speaker, Time Domain Corporation, Huntsville, AL, June 7, 2001.

- R. A. Scholtz, Seminar speaker, Information Sciences Institute, Marina del Rey, CA, September 6, 2001.
- R. A. Scholtz "Remarks on Ultrawideband Radio," first academic speaker at the NETEX Program Industry Day, (a DARPA meeting), McLean VA, Sept. 10, 2001.
- R. A. Scholtz, Speaker and Session Chairman at the Third IEEE Workshop on WLAN, Newton MA, Sept. 27-28, 2001.
- R. A. Scholtz, "Ultrawideband Radio," opening technical speaker at the Intel Ultra-Wideband Technical Forum, Hillsboro, OR, October 11-12, 2001.
- R. A. Scholtz, "Ultrawideband Radio," seminar speaker, Magis Networks, San Diego CA, February 15, 2002.
- R. A. Scholtz, Panelist, "Ultra-wideband - The Future of Short and Medium Range Wireless Communications," WCNC 2002, Orlando, Florida, March 17-21, 2002.
- R. A. Scholtz (woekshop organizer) "An Ultra-Wideband Technology Workshop: From Research to Reality," and Panel Chair "UWB Interference and Coexistence," (jointly sponsored by Intel and the UWB MURI) October 3-4, 2002.
- Ultrawideband Radio: Past, Present, and Future," Berkeley Wireless Research Center Winter Retreat, Monterey CA, January 13-14, 2003.

Graduate students supported by this grant:

Sachin Agrawal
Carlos Corrada, Graduated, Now teaching at the University of Puerto Rico, Rio Piedras campus
Yi-Ling Chao
Yenming Chen
Joon -Yong Lee, Graduated, now teaching at Handong University, Korea.
Robert Weaver

Undergraduate students supported:

Phil Hirz

Miscellaneous information:

In 2001 Dr. Scholtz received the Military Communications Conference Award for Technical Achievement, an award for lifetime contributions to the field, and to this conference in particular.

In 2002-3, Dr. Scholtz served as a consultant to the Defense Science Board Task Force on Wideband RF Technologies.

Ranging in a Dense Multipath Environment Using an UWB Radio Link

Joon-Yong Lee and Robert A. Scholtz, *Life Fellow, IEEE*

***Abstract*—A time-of-arrival (ToA)-based ranging scheme using an ultra-wideband (UWB) radio link is proposed. This ranging scheme implements a search algorithm for the detection of a direct path signal in the presence of dense multipath, utilizing generalized maximum-likelihood (GML) estimation. Models for critical parameters in the algorithm are based on statistical analysis of propagation data and the algorithm is tested on another independent set of propagation measurements. The proposed UWB ranging system uses a correlator and a parallel sampler with a high-speed measurement capability in each transceiver to accomplish two-way ranging between them in the absence of a common clock.**

***Index Terms*—Delay estimation, distance measurement, multipath channels, ultra-wideband (UWB).**

I. Introduction

THE FINE time resolution of ultra-wideband (UWB) signals enables potential applications in high-resolution ranging. The novel aspect of UWB ranging is the fact that the multipath time-spread in many channels of interest is often 100 to 1000 times the inherent time resolution of the UWB signal detected in a matched-filter receiver. Detection of the direct path signal in the presence of dense multipath, which determines ranging quality, becomes a different kind of problem in this case. Multipath resolution techniques in narrowband systems have been well developed [8], [9]. Win and Scholtz [2] introduced a maximum-likelihood (ML) detector for multipath in UWB propagation measurements and Cramer *et al.* [4]–[6] used the CLEAN algorithm to develop a UWB channel model involving angle-of-arrival (AoA), as well as time-of-arrival (ToA).

This paper introduces a ToA measurement algorithm utilizing generalized maximum-likelihood (GML) estimation for the detection of the direct-path signal. Multipath delay and amplitude parameters appearing in this algorithm are modeled statistically from propagation data and the algorithm is tested on an independent set of propagation measurements. Probabilistic analysis of different kinds of errors using these statistical models provides a way of determining the thresholds used in the ToA algorithm, as well as estimating the algorithm's performance. We conclude by presenting the schematic design of an UWB ranging system with a high-speed measurement capability and a two-way ranging technique that utilizes this algorithm.

Manuscript received December 14, 2001. This work was supported by the Office of Naval Research under Contract N00014-00-0221.

J.-Y. Lee was with the Ultra-Wideband Radio Laboratory, University of Southern California, Los Angeles, CA 90089-2560 USA. He is now with School of Computer Science & Electrical Engineering, Handong Global University, Pohang, Korea (e-mail: joonlee@handong.edu).

R. A. Scholtz is with the Communications Sciences Institute, Department of Electrical Engineering–Systems, University of Southern California, Los Angeles, CA 90089-2565 USA (email: scholtz@usc.edu).

Digital Object Identifier 10.1109/JSAC.2002.805060

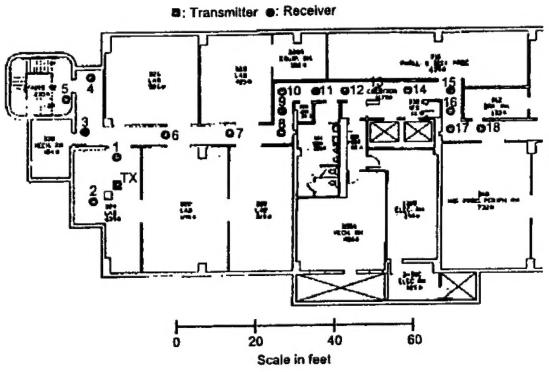

Fig. 1. Basement floor plan of the building where the experiments were conducted. Interior walls are metal stud and dry wall construction. Circular marks stand for the locations of the receiving antenna and the rectangular mark indicates the transmitting antenna's location.

II. Propagation Measurement

A set of indoor propagation measurements was conducted at the University of Southern California to test the ToA algorithm presented in the next section. Pulses with a subnanosecond width were transmitted with one microsecond spacing and measured with a digital sampling scope. The antennas were vertically polarized diamond dipoles [10], approximately 5 ft above the floor. The sampling rate of the measured signal is 20.5 GHz. Sampled waveforms were averaged over 512 sweeps to acquire a higher signal-to-noise ratio (SNR).

Fig. 1 is the floor plan of the building where the measurements were taken. Signals were measured at 18 different locations while the transmitter was fixed in the laboratory. At location 1, the signal was measured with a visually clear line-of-sight (LoS) and used to calibrate the arrival time of the direct path signal. The other 17 signals were measured with a blocked LoS. At locations 16–18, the LoS path was blocked by an elevator (a metallic structure), so the direct path signal could not be measured while multipath could be observed.

Fig. 2 shows the samples of signals taken at location 1, 4, and 14, respectively. Notice that the signals shown in the second and the third plot have stronger multipath components than the direct path signal. In these cases, if a ranging system synchronizes with the strongest signal component for the purpose of range estimation, a large-scale error will occur. The presence of reflected signals that are stronger than the direct path signal makes ranging to the full capabilities of UWB signals challenging.

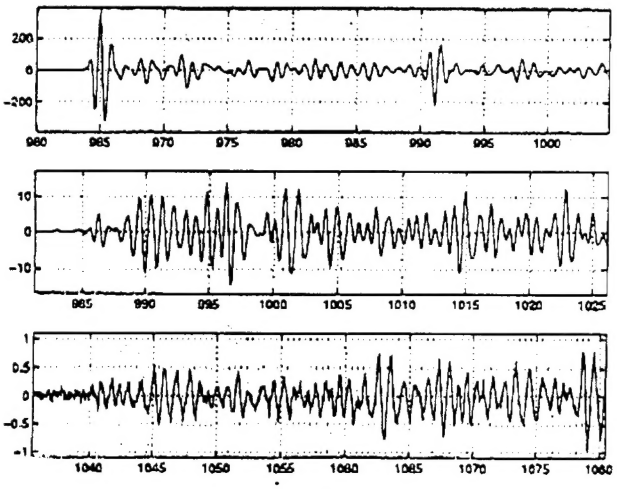

Fig. 2. Measured signals at location 1, 4, and 14. The vertical axis indicates signal strength in millivolts. The vertical scales of each plot are different, indicating differences in channel attenuation. The signal shown in the first plot was measured with a clear LoS and the others were measured in the presence of LoS blockages.

III. Detection of Direct Path Signals

In this paper, the direct path signal is assumed to be the earliest arrival at the receiver. When the straight-line path from transmitter to receiver is in fact a viable propagation path, ToA estimation of the direct path signal is useful for ranging. As shown in the signals of Fig. 2, the direct path signal is not always the strongest in the presence of a visual LoS blockage. The ToA algorithm in this section does not assume that the direct path always supplies the strongest response.

A. Signal Representation

When a single pulse is transmitted, the received signal is composed of direct path signal, reflected signals, noise, and interference [1]. So the received signal $r_m(t)$ can be represented by

$$r_m(t) = a_d s(t-\tau_d) + \sum_{n=1}^{L} a_n s(t-\tau_n) + n_m(t) \quad (1)$$

where $\tau_d < \tau_1 < \tau_2 < \cdots < \tau_L$. The parameters τ_d and a_d are the arrival time and strength of the direct path signal, respectively, and τ_n and a_n are those of the nth reflected component. The waveform $s(t)$ denotes the canonical single-path signal, used as a correlator template, with a width of T_p seconds. The number of multipath signals L is unknown *a priori*. The noise $n_m(t)$ is assumed to be additive white Gaussian, and interference is assumed to be zero.

Let τ_{peak} and a_{peak} be the arrival time and amplitude of the strongest path and assume these have been determined by correlation. Then, $r_s(t)$, a normalized and shifted version of $r_m(t)$, can be represented by

$$\begin{aligned} r_s(t) &= \frac{1}{|a_{peak}|} r_m(t+\tau_{peak}) \\ &= \rho_d s(t+\delta) + \sum_{n}^{L} \alpha_n s(t+\beta_n) + n_s(t) \quad (2) \\ &= \rho_d s(t+\delta) + \sum_{\beta_n \geq 0} \alpha_n s(t+\beta_n) \\ &\quad + \sum_{\beta_n < 0} \alpha_n s(t+\beta_n) + n_s(t) \quad (3) \end{aligned}$$

where

$$\begin{cases} \delta = \tau_{peak} - \tau_d, & \delta \geq 0 \\ \rho_d = a_d/|a_d|, & -1 \leq \rho_d \leq 1 \\ \beta_n = \tau_{peak} - \tau_n, & \delta > \beta_1 > \beta_2 > \cdots > \beta_L \\ \alpha_n = a_n/|a_d|, & -1 \leq \alpha_n \leq 1, \ \forall n \leq L. \end{cases} \quad (4)$$

The noise $n_s(t)$ being a time-shifted version of $n_m(t)$, is a white Gaussian noise signal. The third term in (3) represents the multipath components which arrive later than the peak path. To simplify the problem, let us restrict our observation to the portion of the signal prior to and including the arrival of the strongest path by truncating $r_s(t)$. Let us define $r(t)$ as

$$\begin{aligned} r(t) &= r_s(t), \qquad t \leq \frac{T_p}{2} \\ &= \rho_d s(t+\delta) + \sum_{\beta_k \geq 0} \alpha_k s(t+\beta_k) + n(t), \qquad t \leq \frac{T_p}{2} \\ &= \rho_d s(t+\delta) + \sum_{k=1}^{M} \alpha_k s(t+\beta_k) + n(t), \qquad t \leq \frac{T_p}{2} \end{aligned} \quad (5)$$

where M is the number of signal components that arrived earlier than the peak component. If M is equal to zero, then $\delta = 0$, $\rho_d = \pm 1$, and the second term in (5) is ignored. The noise $n(t)$ is white Gaussian noise [truncated to the interval $(-\infty, T_p/2)$], whose correlation function is represented by

$$R_N(\tau) = \sigma_A^2 \cdot \delta_D(\tau). \quad (6)$$

Assuming $r(t)$ is sampled, let us represent it as a vector of samples, namely

$$\underline{r} = \rho_d \underline{s}_\delta + \sum_{k=1}^{M} \alpha_k \underline{s}_{\beta_k} + \underline{n} \quad (7)$$

where $\underline{s}_\beta$ represents the vector of samples of $s(t+\beta)$ with a same length as $\underline{r}$. The noise vector $\underline{n}$ is a white Gaussian vector whose correlation matrix R_N is given by

$$R_N = \sigma_N^2 \cdot I \quad (8)$$

I being an identity matrix.

B. ToA Measurement Algorithm Using GML Estimation

In (7), δ is the parameter to be estimated and ρ_d, M, $\underline{\alpha}^M$, and $\underline{\beta}^M$ are nuisance parameters, where $\underline{\alpha}^M$ and $\underline{\beta}^M$ are defined as

$$\underline{\alpha}^M = (\alpha_1, \alpha_2, \ldots, \alpha_M) \quad (9)$$

$$\underline{\beta}^M = (\beta_1, \beta_2, \ldots, \beta_M). \quad (10)$$

GML estimation treats all of these unknown parameters as deterministic and estimates δ to be

$$\hat{\delta} = \arg\max_{\delta} \left[\max_{\rho_d, M, \underline{\alpha}, \underline{\beta}} f\left(\underline{r} | \delta, \rho_d, M, \underline{\alpha}^M, \underline{\beta}^M\right) \right]. \quad (11)$$

Because $\underline{n}$ is a white Gaussian vector, this is equivalent to

$$\hat{\delta} = \arg\min_{\delta} \left[\min_{\rho_d, M, \underline{\alpha}, \underline{\beta}} \left\| \underline{r} - \rho_d \underline{s}_\delta - \sum_{k=1}^{M} \alpha_k \underline{s}_{\beta_k} \right\|^2 \right]. \quad (12)$$

Using (12) to estimate δ is computation intensive because $2(M+1)$ unknown parameters are involved. To reduce computational complexity, an iterative nonlinear programming technique is employed, by which the unknown parameters are estimated in a sequential manner [2]. Specifically, the arrival time of each component signal is estimated individually while all other parameters are fixed.

Modification of the estimation criterion shown in (12) is done as follows. First, the duration of the search region for the time δ of arrival of the direct path signal is limited to prevent the probability of a false detection in the noise only portion of the observed signal from becoming too large. We define θ_δ as a limiting threshold on δ so that the direct path signal is searched over the portion of $r(t)$ satisfying $t \geq -\theta_\delta$. Second, a stopping rule is used to terminate the search, because the value of the norm in (12) generally continues to decrease with increasing M. The stopping rule consists of applying a threshold on the relative path strength ρ which is defined as

$$\rho = |\rho_d|. \quad (13)$$

The iterative search process stops when no more paths satisfying $\rho \geq \theta_\rho$ are detected in the search region, where θ_ρ is the threshold of ρ. Third, we skip the estimation of some nuisance parameters by ignoring the multipath components that arrive later than already detected paths. By doing this, we can speed up the search process. Following is a brief description of the ToA algorithm.

1) Let $n = 1$, $\omega_1 = 0$, and $\mu_{11} = 1$.
2) Increase n by 1.
3) Find ω_n which satisfies

$$\omega_n = \arg\max_{\omega_{n-1} < \omega < \theta_\delta} \left(\underline{r} - \sum_{i=1}^{n-1} \mu_{(n-1)i} \underline{s}_{\omega_i} \right)^t \underline{s}_\omega \quad (14)$$

4) Find $(\mu_{n1}, \mu_{n2}, \ldots, \mu_{nn})$ such that

$$(\mu_{n1}, \mu_{n2}, \ldots, \mu_{nn}) = \arg\min_{\mu'_1, \ldots, \mu'_2} \left\| \underline{r} - \sum_{i=1}^{n} \mu'_i \underline{s}_{\omega_i} \right\|^2. \quad (15)$$

5) If $\mu_{nn} \geq \theta_\rho$, go to step 2. Otherwise, proceed to the next step.
6) δ is estimated as $\hat{\delta} = \omega_{n-1}$.

IV. Statistical Modeling of Ranging Parameters

The thresholds θ_δ and θ_ρ, which are used in the ToA algorithm have to be determined so that they satisfy a given performance criteria. One of the potential criteria is that the probability of error is minimized. For the purpose of error analysis, the parameters $\boldsymbol{\delta}$ and $\boldsymbol{\rho}$ which were defined in Section III-A were modeled statistically.

A set of propagation data taken by Win [3] in an office building was used for this modeling. The values of δs and

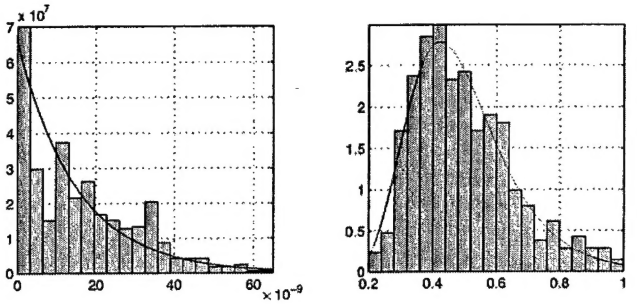

Fig. 3. Normalized histograms of (a) $\boldsymbol{\delta}$ and (b) $\boldsymbol{\rho}$ and approximation of marginal densities using curve-fitting.

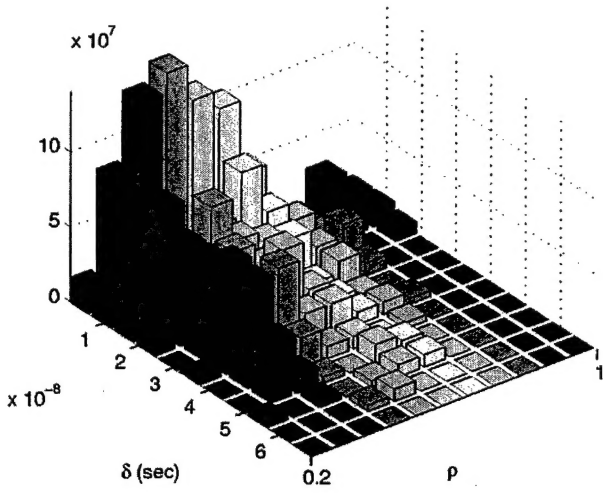

Fig. 4. Histogram of $\boldsymbol{\rho}$ and $\boldsymbol{\delta}$. Total volume was normalized to one.

ρs of 622 signals which were measured with a blocked LoS were extracted using the ToA algorithm. The values of θ_δ and θ_ρ used in this process were 70 ns and 0.2, respectively. Some large scale errors relative to the approximately known distance information were corrected by manually adjusting the thresholds. In 95 of 622 observed signals, the direct path signal was the strongest. So if we define P_0 as the probability that $\boldsymbol{\delta}$ is equal to zero, it can be modeled by

$$P_0 = \Pr(\boldsymbol{\delta} = 0) = \Pr(\boldsymbol{\rho} = 1) = 0.1527. \quad (16)$$

Fig. 3(a) and (b) are normalized histograms of $\boldsymbol{\delta}$ and $\boldsymbol{\rho}$ which were produced with 527 signals that have a stronger reflected path than the direct path. By curve fitting on this data, marginal densities of $\boldsymbol{\delta}$ and $\boldsymbol{\rho}$ can be modeled by

$$f_{\boldsymbol{\delta}}(\delta | \boldsymbol{\delta} \neq 0) = \frac{1}{\sigma_\delta} e^{-\delta/\sigma_\delta}, \qquad \delta > 0 \quad (17)$$

$$f_{\boldsymbol{\rho}}(\rho | \boldsymbol{\rho} \neq 1) = \frac{1}{\sqrt{2\pi} Q(-\mu_\rho/\sigma_\rho) \sigma_\rho \rho} e^{-(\ln \rho - \mu_\rho)^2 / 2\sigma_\rho^2}, \qquad 0 < \rho < 1 \quad (18)$$

where $\sigma_\delta = 1.524 \times 10^{-8}$, $\sigma_\rho = 0.3220$, and $\mu_\rho = -0.7565$. The Q-function appearing in (18) is for normalization.

Independence between $\boldsymbol{\delta}$ and $\boldsymbol{\rho}$ was tested using a chi-squared test. Chi-squared test uses the contingency data set of categorical variables [13], [14]. Fig. 4 is the normalized histogram of δ

and ρ. Pearson's statistic χ^2 with 100 degrees of freedom, which was evaluated with the data set, is 117.2. According to the χ^2 distribution table, the critical value corresponding to a 10% significance level and 100 degrees of freedom is 118.5, which is greater than the value evaluated with data. So we can accept the hypothesis of independence between δ and ρ with a 10% significance level. Based on this result, the joint density of δ and ρ can be modeled by

$$\begin{aligned} &f_{\delta\rho}(\delta,\ \rho|\delta\neq 0,\ \rho\neq 1)\\ &\quad = f_\delta(\delta|\delta\neq 0)\cdot f_\rho(\rho|\rho\neq 1)\\ &\quad = \frac{1}{\sqrt{2\pi}Q(-\mu_\rho/\sigma_\rho)\sigma_\delta\sigma_\rho\rho}\exp\left\{-\left[\frac{\delta}{\sigma_\delta}+\frac{(\ln\rho-\mu_\rho)^2}{2\sigma_\rho^2}\right]\right\} \end{aligned} \tag{19}$$

where $\delta > 0$ and $0 < \rho < 1$.

V. Error Analysis

Range estimation error can result from two major sources. One is ToA estimation error, and the other is any unknown propagation delay in a LoS blockage structure, which is difficult to estimate without a more thorough knowledge of the blockage. In this section, errors in ToA estimation of the direct path signal are analyzed probabilistically.

We can classify ToA errors into two categories. One is early false alarms which occur when a false detection in the noise-only portion of the signal is regarded as that of direct path signal. The other is a missed direct-path error, which occurs when the actual direct path signal is missed and a multipath signal is falsely declared to be direct path signal.

A. Probability of an Early False Alarm

An early false alarm probability P_{FA} can be expressed as

$$\begin{aligned} P_{FA} &= \Pr\left\{\sup_{\beta\in[-\theta_\delta,\,-\delta-T_p)}\frac{|\underline{n}^t\underline{s}_\beta|}{\|\underline{s}_0\|^2} > \theta_\rho \text{ and } \delta\le\theta_\delta - T_p\right\}\\ &= \int_0^{\theta_\delta}\Pr\left\{\sup_{\beta\in[-\theta_\delta,\,-\delta-T_p)}\frac{|\underline{n}^t\underline{s}_\beta|}{\|\underline{s}_0\|^2} > \theta_\rho\right\}\\ &\quad\cdot f_\delta(\delta|\delta\neq 0)\,d\delta\cdot(1-P_0)\\ &\quad+\Pr\left\{\sup_{\beta\in[-\theta_\delta,\,-T_p)}\frac{|\underline{n}^t\underline{s}_\beta|}{\|\underline{s}_0\|^2} > \theta_\rho\right\}\cdot P_0\\ &= \int_0^{\theta_\delta}\Pr\left\{\sup_{\beta\in[-\theta_\delta,\,-\delta-T_p)}\frac{|\underline{w}^t\underline{s}_\beta|}{\|\underline{s}_0\|^2} > \frac{\theta_\rho}{\sigma_N}\right\}\\ &\quad\cdot f_\delta(\delta|\delta\neq 0)d\delta\cdot(1-P_0)\\ &\quad+\Pr\left\{\sup_{\beta\in[-\theta_\delta,\,-T_p)}\frac{|\underline{w}^t\underline{s}_\beta|}{\|\underline{s}_0\|^2} > \frac{\theta_\rho}{\sigma_N}\right\}\cdot P_0 \end{aligned} \tag{20}$$

where

$$\underline{w} = \frac{1}{\sigma_N}\underline{n}. \tag{21}$$

Let us define the peak SNR as the ratio of the peak signal power to the noise power. This can be expressed as

$$\mathrm{SNR}_p = \frac{1}{\sigma_N^2} \tag{22}$$

because the signal was normalized to its peak strength. Substituting (22) into (20)

$$\begin{aligned} P_{FA} &= \int_0^{\theta_\delta}\Pr\left\{\sup_{\beta\in[-\theta_\delta,\,-\delta-T_p)}\frac{|\underline{w}^t\underline{s}_\beta|}{\|\underline{s}_0\|^2} > \theta_\rho\sqrt{\mathrm{SNR}_p}\right\}\\ &\quad\cdot f_\delta(\delta|\delta\neq 0)d\delta\cdot(1-P_0)\\ &\quad+\Pr\left\{\sup_{\beta\in[-\theta_\delta,\,-T_p)}\frac{|\underline{w}^t\underline{s}_\beta|}{\|\underline{s}_0\|^2} > \theta_\rho\sqrt{\mathrm{SNR}_p}\right\}\cdot P_0. \end{aligned} \tag{23}$$

Let us define γ and a random process $u(\beta)$ as

$$\gamma = \theta_\rho\cdot\sqrt{\mathrm{SNR}_p} \tag{24}$$

$$u(\beta) = \frac{|\underline{w}^t\underline{s}_\beta|}{\|\underline{s}_0\|^2}. \tag{25}$$

Substituting (24) and (25) into (23)

$$\begin{aligned} P_{FA} &= \int_0^{\theta_\delta}\Pr\left\{\sup_{\beta\in[-\theta_\delta,\,-\delta-T_p)}u(\beta)>\gamma\right\}f_\delta(\delta|\delta\neq 0)\,d\delta\\ &\quad\cdot(1-P_0)+\Pr\left\{\sup_{\beta\in[-\theta_\delta,\,-T_p)}u(\beta)>\gamma\right\}\cdot P_0. \end{aligned} \tag{26}$$

$\Pr\{\sup_{\beta\in[-\theta_\delta,\,-\delta-T_p)}u(\beta) > \gamma\}$ can be modeled as a high level crossing probability of a random process $u(\beta)$ at a level γ in a given time period $[-\theta_\delta,\ -\delta - T_p)$. This probability can be approximated by [11]

$$\Pr\left\{\sup_{\beta\in[-\theta_\delta,\,-\delta-T_p)}u(\beta)>\gamma\right\}\approx 1-e^{-(\theta_\delta-\delta-T_p)/E(\lambda)} \tag{27}$$

where λ represents the time between a down-crossing and the next adjacent up-crossing at a given level γ. The expected value of λ was simulated using a computer generated white Gaussian vector. The value of λ for a given γ was observed over 100 occurrences and averaged. By curve-fitting on the simulation result, $E(\lambda)$ can be modeled by

$$E(\lambda) = C\cdot e^{B\gamma} \tag{28}$$

where $B = 6.5757$ and $C = 1.375\times 10^{-11}$. Substituting (28) into (27)

$$\begin{aligned} &\Pr\left\{\sup_{\beta\in[-\theta_\delta,\,-\delta-T_p)}u(\beta)>\gamma\right\}.\\ &\qquad = 1-\exp\left[-\frac{(\theta_\delta-\delta-T_p)}{C}e^{-B\gamma}\right]. \end{aligned} \tag{29}$$

Substituting (17) and (29) into (26), we get

$$\begin{aligned} P_{FA} &= 1-(1-P_0)\frac{\sigma_\delta e^{-(\theta_\delta-T_p)/\sigma_\delta}}{\sigma_\delta - Ce^{B\gamma}}\\ &\quad-\frac{P_0\sigma_\delta - Ce^{B\gamma}}{\sigma_\delta - Ce^{B\gamma}}\exp\left[-\frac{(\theta_\delta-T_p)}{C}e^{-B\gamma}\right]. \end{aligned} \tag{30}$$

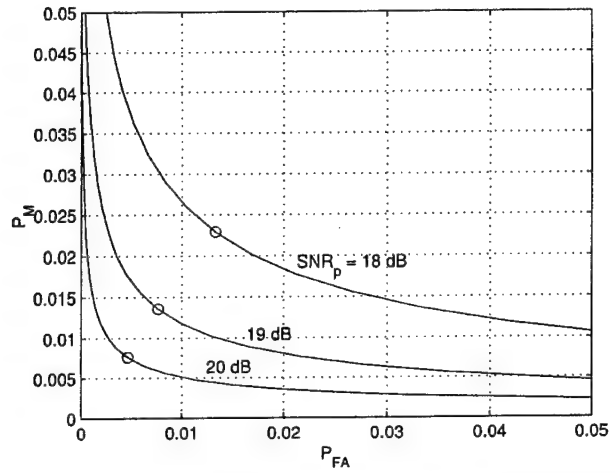

Fig. 5. Early false alarm probability versus probability of a missed direct path for different peak SNRs. $\theta_\delta = 100$ ns and θ_ρ was varied. At the circular mark on each curve, probability of error is minimized.

Substituting (24) into (30)

$$P_{\mathrm{FA}} = 1 - (1 - P_0)\frac{\sigma_\delta e^{-(\theta_\delta - T_{\mathrm{p}})/\sigma_\delta}}{\sigma_\delta - Ce^{B\theta_\rho\sqrt{\mathrm{SNR_p}}}} - \frac{P_0\sigma_\delta - Ce^{B\theta_\rho\sqrt{\mathrm{SNR_p}}}}{\sigma_\delta - Ce^{B\theta_\rho\sqrt{\mathrm{SNR_p}}}} \cdot \exp\left[-\frac{(\theta_\delta - T_{\mathrm{p}})}{C}e^{-B\theta_\rho\sqrt{\mathrm{SNR_p}}}\right]. \quad (31)$$

B. Probability of a Missed-Direct-Path Error

The probability P_{M} of a missed-direct-path error can be evaluated by computing

$$\begin{aligned} P_{\mathrm{M}} &= \Pr(\boldsymbol{\delta} > \theta_\delta \text{ or } \boldsymbol{\rho} < \theta_\rho) \\ &= 1 - \Pr(0 \le \boldsymbol{\delta} \le \theta_\delta \text{ and } \theta_\rho \le \boldsymbol{\rho} \le 1) \\ &= 1 - P_0 - (1 - P_0)\int_{\theta_\rho}^{1}\int_{0}^{\theta_\delta} f_{\boldsymbol{\delta\rho}}(\delta, \rho | \boldsymbol{\delta} \ne 0)\, d\delta\, d\rho. \end{aligned} \quad (32)$$

Substituting (19) into (32)

$$P_{\mathrm{M}} = (1 - P_0)\left[1 - \left(1 - e^{-\theta_\delta/\sigma_\delta}\right)\left(1 - \frac{Q\left(\frac{\ln\theta_\rho - \mu_\rho}{\sigma_\rho}\right)}{Q\left(\frac{-\mu_\rho}{\sigma_\rho}\right)}\right)\right]. \quad (33)$$

Fig. 5 is a plot of P_{FA} versus P_{M} for different values of peak SNR. The value of θ_δ was fixed at 100 ns and these two error probabilities were calculated for various θ_ρ. The circular mark on each curve represents the points where the sum of the two error probabilities is minimized.

VI. Test on Measured Data

Fig. 6 shows of test results of the ToA algorithm on the signals measured at location 9 and 13. In each example, the upper plot is the measured waveform and the lower one shows the reconstructed signal with the paths detected in the ToA algorithm. The value of θ_ρ was determined so that the total probability of error ($P_{\mathrm{FA}} + P_{\mathrm{M}}$) is minimized while θ_δ was fixed. The vertical line appearing in each plot indicates the expected arrival time of the direct-path signal in the presence of a clear LoS path, based on physical range measurements. We can observe a few nanoseconds of discrepancy between this line and signal frontend in both examples. This probably is caused by excessive propagation delay in the LoS blockage. This unknown delay makes it difficult to measure the true arrival time of direct path.

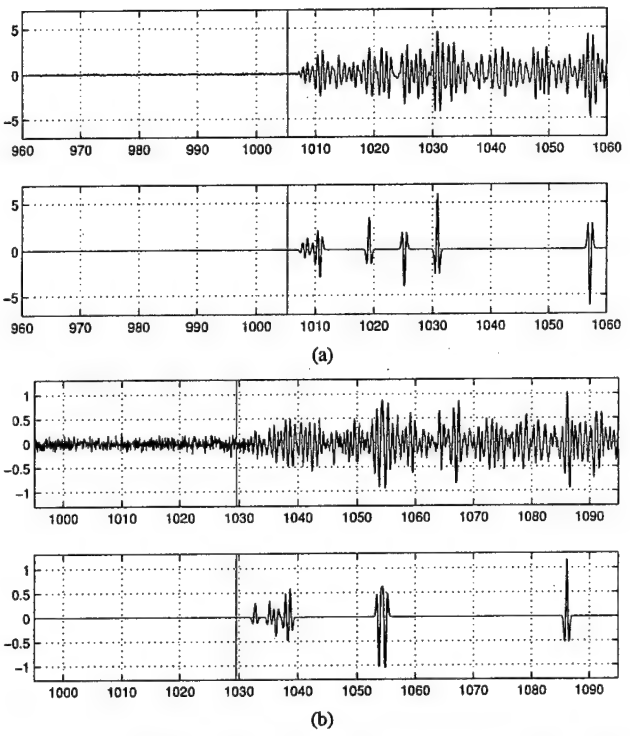

Fig. 6. ToA algorithm tested on measured signal at location 9 and 13. The vertical scale is in millivolts. Vertical line in each plot show the ToA of the direct path signal based on true measured range, assuming the presence of a clear LoS. $\theta_\delta = 100$ ns and θ_ρ was determined so that $P_{\mathrm{FA}} + P_{\mathrm{M}}$ is minimized. The values of θ_ρ used in each test are (a) 0.050 and (b) 0.154.

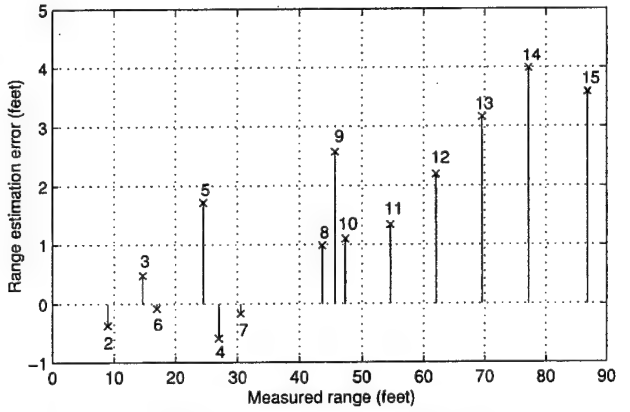

Fig. 7. Range estimation errors (estimated range–measured range). The numbers are the index of measurement positions. Ranging errors shown in this plot contains excessive propagation delay in the blockage structures.

Fig. 7 shows the range estimation errors incurred in this test at the locations marked in Fig. 1. Notice that larger errors occurred

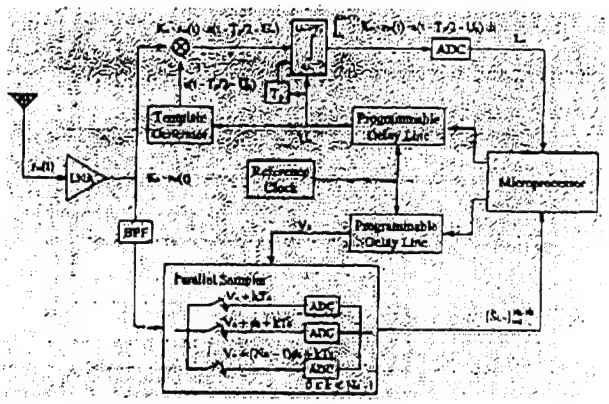

Fig. 8. Receiver schematic of UWB ranging system.

at long ranges, probably because the structure of LoS blockage was more complex at these locations.

VII. Design of UWB Ranging System

A. System Description

Withington *et al.* [7] introduced an UWB scanning receiver system which, using two correlators, has the capability of communication and channel pulse response measurement. The block diagram of an UWB ranging system using a correlator and a parallel sampler is shown in Fig. 8. When the signal is received, the correlator synchronizes with the signal, U_n being the time-tracking point in the nth time frame. Once the correlator is locked, the parallel sampler starts sampling the incoming signal under the time control of a trigger signal. The trigger time V_n in the nth time frame is controlled relative to the tracking time U_n. This parallel sampler is composed of a bank of N_R individual samplers and N_R analog-to-digital converters (ADC). Each individual sampler takes N_S samples per time frame at a sampling rate of $1/T_S$ Hz. The offset in the sampling times of two adjacent individual samplers is ϕ_s, which satisfies

$$\phi_s \cdot N_R = T_S. \tag{34}$$

Total $N_S \cdot N_R$ samples are taken in each time frame by this parallel sampler and the overall sampling frequency is $1/\phi_s$ Hz. To acquire an acceptable SNR, each sample is integrated over several time frames. By changing the sampler's trigger time relative to the time-tracking point, the sampling frequency of the measured signal can be increased.

B. Two-Way Ranging Scheme

A UWB ranging system estimates the range by measuring signal round-trip time without a common timing reference. This ranging scheme uses a two-way remote synchronization technique [12] employed in satellite systems. Fig. 9 is the timing diagram of this approach. A pair of UWB radios are time multiplexed with a period of T_M. Each radio switches between a transmission mode and a reception mode every $T_M/2$ s. Radio 1 transmits signal 1, which is a train of pulses without modulation. It is received by radio 2 and signal 1′ denotes the captured signal. The time-multiplex period T_M is assumed to be large

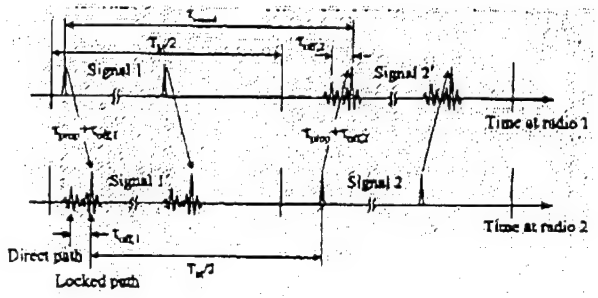

Fig. 9. Evaluation of the signal round-trip time.

enough relative to the temporal profile of the received signal so that it does not affect the next transmission. The delay between transmission and reception of this signal is $\tau_{prop} + \tau_{off,1}$, where τ_{prop} is the propagation time, and $\tau_{off,1}$ represents the time offset between the locked path and the direct path. With a known delay of $T_M/2$ from the front end of signal 1′, radio 2 transmits signal 2 and it is captured by radio 1. Signal 2′ denotes the captured signal by radio 1. Similarly, a delay of $\tau_{prop} + \tau_{off,2}$ exists in this direction. The structures of signal 2 and signal 2′ are similar to those of signal 1 and signal 1′, respectively. Radio 1 can measure the signal round-trip time, τ_{round}, which is

$$\tau_{round} \approx 2\tau_{prop} + \frac{T_M}{2} + \tau_{off,1} + \tau_{off,2}. \tag{35}$$

Then, the signal propagation time can be approximated by

$$\tau_{prop} \approx \frac{\tau_{round} - T_M/2 - \tau_{off,1} - \tau_{off,2}}{2}. \tag{36}$$

Radio 2 informs radio 1 of $\tau_{off,1}$ afterwards with a few bits of information so that radio 1 can evaluate the signal propagation time. If the SNR of the measured signal is not large enough, the two radios increase the signal measurement time to acquire an acceptable SNR.

VIII. Conclusion

According to tests on the propagation data, there exists excessive propagation delay in the LoS blockage material which is considerable when the structure of this blockage is complex. This excessive propagation delay is a limiting factor in UWB ranging performance through materials.

Acknowledgment

The authors would like to thank Prof. K. Chugg and Prof. U. Mitra for their suggestions.

References

[1] R. A. Scholtz *et al.*, "UWB radio deployment challenges," in *Proc. Personal, Indoor Mobile Radio Communications (PIMRC 2000)*, vol. 1, 2000, pp. 620–625.

[2] M. Z. Win and R. A. Scholtz, "Energy capture versus correlator resources in ultra-wide bandwidth indoor wireless communications channels," in *Proc. Milcom*, vol. 3, Nov. 1997, pp. 1277–1281.

[3] ——, "Ultra-wide bandwidth signal propagation for indoor wireless communications," in *Proc. ICC*, June 1997.

[4] J. M. Cramer, R. A. Scholtz, and M. Z. Win, "Spatio–temporal diversity in ultra-wideband radio," in *Proc. WCNC*, vol. 2, 1999, pp. 888–892.

[5] J. M. Cramer, M. Z. Win, and R. A. Scholtz, "Evaluation of multipath characteristics of the impulse radio channel," in *Proc. PIMRC*, vol. 2, 1998, pp. 864–868.
[6] J. M. Cramer, R. A. Scholtz, and M. Z. Win, "Evaluation of an ultra-wideband propagation channel," *IEEE Trans. Antennas Propagat.*, vol. 50, pp. 561–570, May 2002.
[7] P. Withington, R. Reinhardt, and R. Stanley, "Preliminary results of an ultra-wideband (impulse) scanning receiver," in *Proc. MILCOM*, vol. 2, 1999, pp. 1186–1190.
[8] T. G. Manickam, R. J. Vaccaro, and D. W. Tufts, "A least-squares algorithm for multipath time-delay estimation," *IEEE Trans. Signal Processing*, vol. 42, pp. 3229–3233, Nov. 1994.
[9] I. Ziskind and M. Wax, "Maximum likelihood localization of multiple sources by alternating projection," *IEEE Trans. Acoust., Speech, Signal Processing*, vol. 36, pp. 1553–1560, Oct. 1988.
[10] H. G. Schantz and L. Fullerton, "The diamond dipole: A Gaussian impulse antenna," in *Proc. IEEE AP-S Int. Symp.*, Boston, MA, July 2001.
[11] J. R. Rice, "First-occurrence time of high-level crossings in a continuous random process," *J. Acoust. Soc. Amer.*, vol. 39, pp. 323–335, 1966.
[12] W. C. Lindsey and M. K. Simon, *Phase and Doppler Measurements in Two-Way Phase-Coherent Tracking Systems*. New York: Dover, 1991.
[13] E. L. Lehmann, *Nonparametrics: Statistical Methods Based on Ranks*. San Francisco, CA: McGraw-Hill, 1975.
[14] P. E. Greenwood and M. S. Nikulin, *A Guide to Chi-Squared Testing*. New York: Wiley, 1975.

Joon-Yong Lee was born in Seoul, Korea, in 1970. He received the B.S. degree in electrical engineering from Hong-Ik University, Seoul, Korea, in 1993, and the M.S. and Ph.D. degrees in electrical engineering from the University of Southern California (USC), Los Angeles, CA, in 1997 and 2002, respectively.

From 1998 to 2002, he was a Research Assistant with the Ultra-Wideband Radio Laboratory (UltraLab), USC. At USC, he worked primarily on the design of UWB ranging systems. His research interests are the characterization of UWB propagation channels and the design of UWB positioning systems. Since 2002, he has been with the School of Computer Science & Electrical Engineering, Handong Global University, Pohang, Korea, as a Faculty Member.

Robert A. Scholtz (S'56–M'59–SM'73–F'80–LF'02) was born in Lebanon, OH, on January 26, 1936. He is a Distinguished Alumnus of the University of Cincinnati, OH, where, as a Sheffield Scholar, he received the E.E. degree in 1958. He was a Hughes Masters and Doctoral Fellow while obtaining the M.S. and Ph.D. degrees in electrical engineering from University of Southern California (USC), Los Angeles, in 1960, and Stanford University, Stanford, CA, in 1964, respectively.

While working on missile radar signal processing problems, he remained part-time at Hughes Aircraft Company until 1978. In 1963, he joined the faculty of the USC, where he is now Professor of electrical engineering. From 1984 to 1989, he served as Director of USC's Communication Sciences Institute. He was Chairman of the Electrical Engineering Systems Department from 1994 to 2000. In 1996, as part of the Integrated Media Systems Center effort, he was instrumental in forming the Ultra-wideband Radio Laboratory (UltRa Lab) to provide facilities for the design and test of impulse radio systems and other novel high-bandwidth high-data-rate wireless mobile communication links. He has consulted for the LinCom Corporation, Axiomatix, Inc., the Jet Propulsion Laboratory, Technology Group, TRW, Pulson Communications (Time Domain Corporation), and Qualcomm, as well as various government agencies. His research interests include communication theory, synchronization, signal design, coding, adaptive processing, and pseudonoise generation, and their application to communications and radar systems. He co-authored *Spread Spectrum Communications* with M. K. Simon, J. K. Omura, and B. K. Levitt and *Basic Concepts in Information Theory and Coding* with S. W. Golomb and R. E. Peile. He has been General Chairman of five workshops in the area of communications, including most recently the Ultrawideband Radio Workshop held in May 1998, and has been an active participant on NSF panels and in research planning workshops of the U.S. Army Research Office.

Dr. Scholtz was elected to the grade of Fellow in the IEEE, "for contributions to the theory and design of synchronizable codes for communications and radar systems" in 1980. In 1983, he received the Leonard G. Abraham Prize Paper Award for the historical article, "The origins of spread spectrum communications;" this same paper received the 1984 Donald G. Fink Prize Award given by the IEEE. His paper "Acquisition of spread-spectrum signals by an adaptive array" with D. M. Dlugos received the 1992 Senior Award of the IEEE Signal Processing Society. His paper "Strategies for minimizing the intercept time in a mobile communication network with directive/adaptive antennas," with J.-H. Oh received the Ellersick Award for the best unclassified paper at Milcom 1997. His paper "ATM based ultrawide bandwidth (uwb) multiple-access radio network for multimedia PCS" with students M. Z. Win, J. H. Ju, X. Qiu, and colleague V. O. K. Li received the best student paper award from the NetWorld+Interop'97 program committee. In 2001, he received the Military Communications Conference Award for Technical Achievement. He has been an active member of the IEEE for many years, manning important organizational posts, including Finance Chairman for the 1977 National Telecommunications Conference, Program Chairman for the 1981 International Symposium on Information Theory, and Board of Governors positions for the Information Theory Group and the Communications Society.

Problems in Modeling UWB Channels

Robert A. Scholtz and Joon-Yong Lee

Abstract— **Ultrawideband (UWB) channel models pose a new set of problems to the designer. The very wide radio-frequency bandwidth employed by a UWB radio means that more structure of the channel is exposed by the fine time-resolution of the UWB radio receiver. Issues pertinent to design and simulation of UWB communication and ranging systems will be illustrated through a set of UWB measurements.**

I. Introduction

THE inherent time resolution (or range resolution) of a signal $s(t)$ can be determined by evaluating the response of a matched filter detector to small time displacements τ of $s(t)$. The ambiguity function provides a plot of the detector output as a function of τ that has a peak at $\tau = 0$, the response when there is no timing error. The width of this peak, which is a measure of time resolution, is inversely proportional to the bandwidth, and hence is very small for ultrawideband signals. Woodward's radar ambiguity function [5] for narrowband signals has two parameters: time mismatch τ and frequency mismatch to account for unknown doppler shifts and oscillator offsets. For a carrierless UWB signal, a similar ambiguity function is defined using time mismatch τ and time-scaling factor α (related to clock offset), this scaling being the source of doppler shift in narrowband signals. It is important that the stability of clocks in UWB systems be good enough to insure that clock jitter is significantly smaller than the resolution of the receiver's detector.

Ranging to the full theoretical capabilities of UWB signals is not a simple task. As bandwidth increases, a single multipath component at low bandwidth may be time-resolved into multiple components, usually each with a smaller level of energy content. Ranging requires that the direct path portion of the signal be located and its arrival time inserted into ranging algorithms. Finding the direct path component among possibly hundreds of resolvable multipath components is signal-processing intensive, especially since the direct path, while earliest in arrival time, may be considerably smaller in amplitude than later arriving components [2], [4]. A time-of-arrival (ToA) measurement algorithm for UWB ranging, which assumes the presence of over-sampled measurement data, was introduced in [4]. In this paper, we suggest a modification of the ToA algorithm to reduce the number of correlation computations (samples) in the direct-path search process, thereby reducing the time to produce a range estimate.

This work was supported by the Office of Naval Research under Contract No. N00014-00-0221.

Robert Scholtz is with the University of Southern California, Los Angeles, CA 90089-2565. e-mail: scholtz@usc.edu.

Joon-Yong Lee is with Handong Global University, Pohang, Korea. e-mail: joonlee@handong.edu.

II. UWB Ambiguity Function

A. Definition

Let's assume that a UWB time-limited signal is transmitted through a free-space channel. Ignoring receiver noise, the received signal $s_{\rm r}(t)$ is of the form

$$s_{\rm r}(t) = A_{\rm r} s\Big(\alpha(t-\tau_{\rm r})\Big), \tag{1}$$

where $A_{\rm r}$ is the amplitude of received signal, $\tau_{\rm r}$ is an time-shift, and α is a time-scale factor. The receiver, not having prior knowledge of $A_{\rm r}$, $\tau_{\rm r}$, and α, constructs a matched-filter/correlator matched to $s_{\rm m}(t)$, which is

$$s_{\rm m}(t) = A_{\rm m} s(t-\tau_{\rm m}), \tag{2}$$

and the matched filter output $z(t)$ is given by

$$\begin{aligned} z(t) &= A_{\rm r}A_{\rm m}\int_{-\infty}^{\infty} s(t-\tau_{\rm m}) s\Big(\alpha(t-\tau_{\rm r})\Big)dt \\ &= \frac{A_{\rm r}A_{\rm m}}{\sqrt{\alpha}}\int_{-\infty}^{\infty} \sqrt{\alpha}s(t) s\Big(\alpha(t-\tau)\Big)dt \end{aligned} \tag{3}$$

where

$$\tau = \tau_{\rm r} - \tau_{\rm m}. \tag{4}$$

The UWB ambiguity function, namely $\chi_{\rm uwb}(\tau,\alpha)$, can be defined as

$$\chi_{\rm uwb}(\tau,\alpha) = \int_{-\infty}^{\infty} \sqrt{\alpha}s(t)s(\alpha(t-\tau))dt, \tag{5}$$

where $\sqrt{\alpha}$ is for normalization so that the signal energy is kept constant. The UWB ambiguity function satisfies

$$\chi_{\rm uwb}(\tau,\alpha) \le \chi_{\rm u}(0,1) = E_{\rm s}, \tag{6}$$

where $E_{\rm s}$ denotes the energy of $s(t)$,

$$E_{\rm s} = \int_{-\infty}^{\infty} |s(t)|^2 dt = \int_{-\infty}^{\infty} |S(f)|^2 df, \tag{7}$$

where $S(f)$ is the Fourier transform of $s(t)$. If α is equal to 1, $\chi_{\rm uwb}(\tau,\alpha)$ can be interpreted as the auto-correlation function of $s(t)$.

The function $\chi_{\rm uwb}(\tau,\alpha)$ can be approximated near $(0,1)$ using the initial terms of a Taylor series expansion.

$$\begin{aligned} \chi_{\rm uwb}(\tau,\alpha) \approx \chi_{\rm uwb}(0,1)\Big[1 + A_\tau\tau + A_\alpha(\alpha-1) + \frac{1}{2}B_\tau\tau^2 \\ + \frac{1}{2}B_\alpha(\alpha-1)^2 + \frac{1}{2}B_{\tau\alpha}\tau(\alpha-1)\Big], \end{aligned} \tag{8}$$

where A_τ, A_α, B_τ, B_α, and $B_{\tau\alpha}$ are defined as

$$\begin{cases} A_\tau &= \dfrac{1}{\chi_{\rm uwb}(0,1)}\dfrac{\partial}{\partial\tau}\chi_{\rm u}(\tau,\alpha)\Big|_{\tau=0,\alpha=1}, \\ A_\alpha &= \dfrac{1}{\chi_{\rm u}(0,1)}\dfrac{\partial}{\partial\alpha}\chi_{\rm uwb}(\tau,\alpha)\Big|_{\tau=0,\alpha=1}, \\ B_\tau &= \dfrac{1}{\chi_{\rm u}(0,1)}\dfrac{\partial^2}{\partial\tau^2}\chi_{\rm uwb}(\tau,\alpha)\Big|_{\tau=0,\alpha=1}, \\ B_\alpha &= \dfrac{1}{\chi_{\rm u}(0,1)}\dfrac{\partial^2}{\partial\alpha^2}\chi_{\rm uwb}(\tau,\alpha)\Big|_{\tau=0,\alpha=1}, \\ B_{\tau\alpha} &= \dfrac{1}{\chi_{\rm u}(0,1)}\dfrac{\partial^2}{\partial\tau\partial\alpha}\chi_{\rm uwb}(\tau,\alpha)\Big|_{\tau=0,\alpha=1}. \end{cases} \tag{9}$$

and evaluated by

$$A_\tau = A_\alpha = 0, \tag{10}$$

$$B_\tau = -\frac{1}{\chi_{\rm uwb}(0,1)}\int_{-\infty}^{\infty}(2\pi f)^2|S(f)|^2df, \tag{11}$$

$$B_\alpha = \frac{1}{\chi_{\rm uwb}(0,1)}\left[-\frac{3E_s}{4}+\int_{-\infty}^{\infty}t^2s(t)s''(t)dt\right], \tag{12}$$

$$B_{\tau\alpha} = -\frac{1}{\chi_{\rm uwb}(0,1)}\int_{-\infty}^{\infty}ts(t)s''(t)dt. \tag{13}$$

Using the fact that $E_s/\chi_{\rm uwb}(0,1)$ integrates to 1, we can relate the Gabor (or rms) bandwidth $B_{\rm rms}$ (in Hertz) of the signal $s(t)$ to B_τ by

$$\frac{B_\tau^{\frac{1}{2}}}{2\pi} = B_{\rm rms} = \left[\int_{-\infty}^{\infty}f^2\frac{|S(f)|^2}{\chi_{\rm u}(0,1)}df\right]^{\frac{1}{2}}. \tag{14}$$

This large value of B_τ for UWB signals makes the shape of the peak of $\chi(\tau,\alpha)$ very narrow as a function of time, thereby justifying the fine time resolution capability of a matched UWB receiver.

B. Computer Plots

UWB ambiguity functions with different formats were evaluated using computer simulations. In these simulations, the received UWB pulse $s(t)$ was assumed to be the second derivative of a gaussian shape, which is given by [3]

$$s(t) = \left[1-4\pi(t/\tau_m)^2\right]\exp\left[-2\pi(t/\tau_m)^2\right], \tag{15}$$

where $\tau_m = 0.781\times10^{-9}$.

Figure 1 shows the ambiguity function of a single UWB pulse. The range of the scale factor α goes well beyond mismatches that which can be caused by radial velocities by transmitter and receiver, and hence the velocity resolution is not very good, while the time resolution is very fine. This ambiguity function of a single UWB pulse can be classified as the knife-edge type.

Suppose the UWB ranging system transmits and receives a train of pulses. Because of the absence of a common clock, there may exist mismatch in the clock periods of the

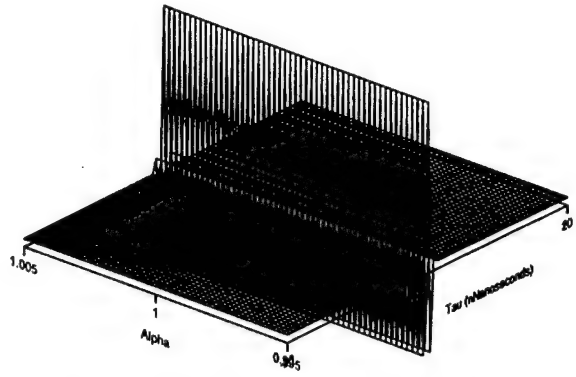

Fig. 1. UWB ambiguity function of a single pulse.

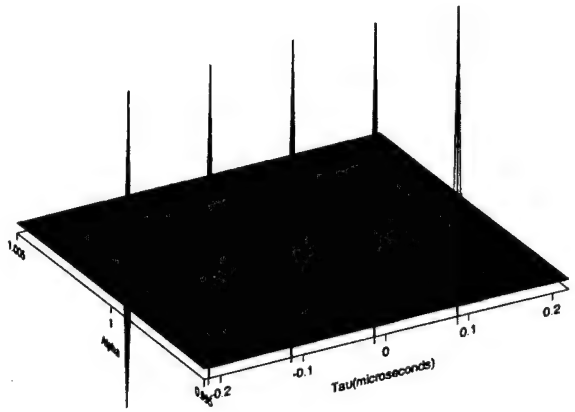

Fig. 2. UWB ambiguity function of a periodic train of 64 pulses. The pulse repetition rate is 10 Mpps.

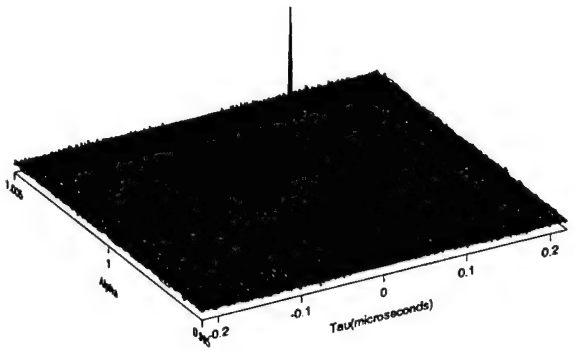

Fig. 3. UWB ambiguity function of 64 time hopped pulses with $N_h = 32$, $T_f = 100$ ns, and $T_c = 2$ ns.

transmitter and receiver. The order of the clock period mismatch can be possibly as large as 0.1% for a very poor clock. Let's assume no pulse-shape distortion, but instead consider the clock period mismatch as the second factor of the UWB ambiguity function. In this case the UWB ambiguity function of a train of N_p periodic pulses can be computed as

$$\chi_\mathrm{u}(\tau,\alpha) = \int_{-\infty}^{\infty} \sum_{i=0}^{N_\mathrm{p}-1} \sum_{j=0}^{N_\mathrm{p}-1} s\left(t - iT_\mathrm{f} + \frac{(N_\mathrm{p}-1)T_\mathrm{f}}{2}\right) \cdot s\left(t - \tau - j\alpha T_\mathrm{f} + \frac{(N_\mathrm{p}-1)T_\mathrm{f}}{2}\right) dt, \quad (16)$$

where T_f is the clock period and α is the scaling factor caused by clock period differences, which is equal to

$$\alpha = \frac{T_\mathrm{f}}{T_\mathrm{f} + T_\mathrm{d}}, \quad (17)$$

where T_d denotes the clock period mismatch. Detailed evaluation of the ambiguity function of the periodic gaussian pulse train is given in [6] and figure 2 is a simulated ambiguity function. The number of pulses was assumed to be 64 and pulse repetition rate is 10 Mpps. We can still measure the range with a fine resolution but with a pulse-repetition-time ambiguity in time mismatch. Figure 3 is the ambiguity function of a train of time hopped pulses, which is represented by

$$\chi_\mathrm{u}(\tau,\alpha) = \int_{-\infty}^{\infty} \sum_{i=0}^{N_\mathrm{p}-1} \sum_{j=0}^{N_\mathrm{p}-1} s\left(t - iT_\mathrm{f} - c_i(u)T_\mathrm{c} + \frac{(N_\mathrm{p}-1)T_\mathrm{f}}{2}\right) \cdot s\left(t - j\alpha T_\mathrm{f} - c_j(u)T_\mathrm{c} + \frac{(N_\mathrm{p}-1)T_\mathrm{f}}{2}\right) dt, \quad (18)$$

where T_f and T_c denote frame time and chip time, respectively. The time hopping sequence $\{c_j(u)\}$ satisfies

$$0 \le c_i(u) \le N_h - 1. \quad (19)$$

It was assumed that $N_\mathrm{p} = 64$, $N_\mathrm{h} = 32$, $T_\mathrm{f} = 100$ ns, and $T_\mathrm{c} = 2$ ns. The time-hopping pattern of the sequence employed here was assumed to be uniform over 32 time bins. Notice that ambiguities along time axis were suppressed down by time-hopping.

III. A System-Friendly Algorithm for UWB Ranging

A. Modification of the ToA Algorithm

The ToA measurement algorithm using generalized maximum likelihood estimation (GML) was introduced in [4]. In this algorithm, the ToA of the direct path signal is estimated using two critical parameters, relative strength and relative time displacement between the strongest path and the potential direct path signal, with over-sampled measurement data. However, in real systems, the measurement time is limited and the sampling frequency may not be high enough to perform the GML estimation.

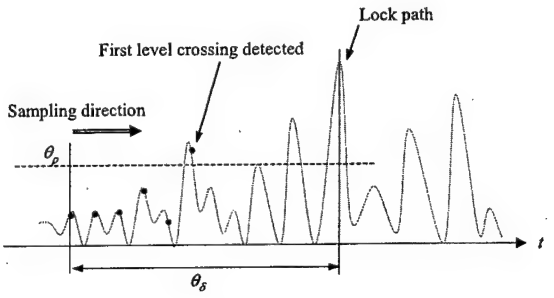

Fig. 4. Search for the earliest arrival of the signal using uniform sampling. Search is performed in a positive direction along the time axis.

The ToA algorithm can be modified in a system-friendly manner as follows. First, the search region for the direct path signal with a given length of θ_δ is set in the forward direction from the location of the locked path instead of the strongest path to reduce the measurement time spent on the peak search. It is difficult to characterize the time displacement between the locked path and the strongest path without a thorough knowledge of the acquisition scheme. However, considering that the acquisition strategy is based on threshold detection, by which the tracking correlator is locked on the first level crossing point at the threshold, we can assume that the correlator is locked on a path which arrives earlier than the peak path. As a consequence, the probability of a false detection in the noise only portion of the signal would increase, while the risk of missing the direct path signal beyond the range of search would decrease. Secondly, the threshold of the amplitude (θ_ρ) is determined only by the noise floor without considering the relative path strength due to the absence of the knowledge of the peak strength. Thirdly, the first level crossing point is regarded as the ToA of direct path signal since computation of GML estimation cannot be done with under-sampled data.

Figure 4 illustrates the search process. Search by sampling is done in the positive direction along the time axis and terminated once the first level crossing is detected.

B. Sampling Issues

To achieve an accurate detection in a limited measurement time, which is determined by sampling rate, length of search region, and the number of pulse periods per measurement, effective sampling design is critical. To determine the sampling strategy, it is necessary to know the minimum sampling frequency required. For example, the larger the distance between two adjacent samples, the higher is the risk of missing the level crossing point between them.

While it is very difficult to evaluate the probability of missing a level crossing between samples, we can think of some ways to measure this risk. One of them is to quantify the interpolation error caused by under-sampling, assuming the signal is deterministic. Since the signal from which

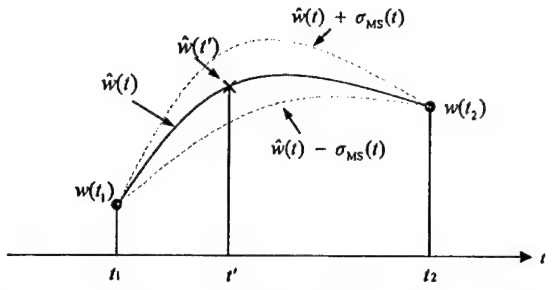

Fig. 5. Reconstruction of signal using MMSE estimation based on two samples. Solid curve indicates the reconstructed signal and the dotted line shows the error deviation.

the samples are taken is not band-limited, it is impossible to sample at the Nyquist rate and as a consequence, perfect signal reconstruction from samples is impossible [7]. The amount of energy in high frequency signal components lost due to aliasing will provide one way of measuring the sampling quality. Another approach is to evaluate the error variance in minimum mean square error (MMSE) estimation, assuming the correlator output signal is a wide sense stationary process. Figure 5 shows an example of MMSE estimation using two samples. In this figure, $\hat{w}(t')$ denotes the MMSE estimate of $w(t')$ evaluated with observation vector of samples, namely $\underline{m}$, which is

$$\underline{m} = \begin{bmatrix} w(t_1) \\ w(t_2) \end{bmatrix}. \tag{20}$$

The solid line represents the reconstructed signal using MMSE estimation and the dotted lines represent one standard deviation of the estimation error. The closer the dotted line is to the threshold level at which the crossing is searched, the larger is the probability of missing the occurrence of a threshold crossing. MMSE estimate of $w(t')$ and the error variance $\sigma^2_{MS}(t')$ are given by

$$\hat{w}(t') = R_{\hat{w}m} R_m^{-1} \underline{m}, \tag{21}$$

$$\sigma^2_{MS}(t') = \mathrm{Tr}\left(R_{\hat{w}} - R_{\hat{w}m} R_m^{-1} R_{m\hat{w}}\right), \tag{22}$$

where $R_{\hat{w}}$ and R_m are correlation matrix $\hat{w}(t')$ and $\underline{m}$, respectively, $R_{\hat{w}m}$ is the cross-correlation matrix of $\hat{w}(t')$ and $\underline{m}$, and $\mathrm{Tr}(\cdot)$ is the trace function. Correlation matrices appearing in (21) are evaluated by computing

$$R_{\hat{w}} = R_w(0), \tag{23}$$

$$R_m = \begin{bmatrix} R_w(0) & R_w(t_1 - t_2) \\ R_w(t_2 - t_1) & R_w(0) \end{bmatrix}, \tag{24}$$

$$R_{\hat{w}m} = [R_w(t' - t_1)\ R_w(t' - t_2)], \tag{25}$$

where $R_w(\tau)$ denotes the auto-correlation function of $w(t)$. As shown in (21) through (25), to calculate $\hat{w}(t')$ and $\sigma^2_{MS}(t')$, auto-correlation function of the correlator output signal must be evaluated.

Figure 6 is the block diagram of a matched filter system which is equivalent to a potential UWB radio link. A

Fig. 6. Transmission and reception of signal in UWB radio link.

transmitted UWB pulse $p(t)$ goes though the channel including antennas whose impulse response is $h_b(t)$, and the resulting output is correlated/match-filtered with the template signal $u(t)$. Assuming the correlator output $w(t)$ is a wide sense stationary random process, the energy spectral density $S_w(f)$ of $w(t)$ can be approximated by

$$S_w(f) = |U(f)|^2 |H_b(f)|^2 S_p(f), \tag{26}$$

where $S_p(f)$ is the energy spectral density of $p(t)$. The channel function $H_b(f)$ can be modeled using the measured antenna system function $H_a(f)$ shown in figure 8, which is

$$H_b(f) = c_a \cdot H_a(f), \tag{27}$$

where the unknown constant c_a is the attenuation factor. The antenna system measurement to evaluate $H_a(f)$ is given in [1]. Let's define $S'_w(f)$ and $R'_w(\tau)$ as

$$S'_w(f) = |U(f)|^2 |H_a(f)|^2 S_p(f), \tag{28}$$

$$R'_w(\tau) = F^{-1}\{S'_w(f)\}. \tag{29}$$

Then, $S_w(f)$ and $R_w(\tau)$ satisfy

$$S_w(f) = c_a^2 \cdot S'_w(f), \tag{30}$$

$$R_w(\tau) = c_a^2 \cdot R'_w(\tau). \tag{31}$$

In figure 7 through figure 10, plots of $S_p(f)$, $|U(f)|^2$, $S'_w(f)$, and $R'_w(\tau)$ are shown. Again, the template $u(t)$ is the second derivative of a gaussian pulse as shown in (15). The unknown constant c_a can be evaluated using (31), which is

$$c_a = \sqrt{\frac{R_w(0)}{R'_w(0)}} = \sqrt{\frac{E_w}{R'_w(0)}}, \tag{32}$$

where E_w is the total energy of $w(t)$. So calculation of c_a requires knowledge of the total energy of $w(t)$, which is difficult to estimate without knowledge of the channel.

Figure 11 and figure 12 are examples of the standard deviation of error, $\sigma_{MS}(t)$, assuming c_a is equal to 1. Figure 11 compares $\sigma_{MS}(t)$ with different sampling rates, assuming the number of samples used for the estimation is 2. Notice that the peak of each curve is located at the midpoint between the two samples. Figure 12 shows another comparison of $\sigma_{MS}(t)$ with a different number of observations used for the estimation, while the sampling rate is fixed at 2 GHz, assuming the closest samples are used for estimation. The error deviation decreases as the number of observations used increases.

IV. Conclusions

Measurement time of the signal is one of the major limiting factors in UWB ranging performance. Furthermore,

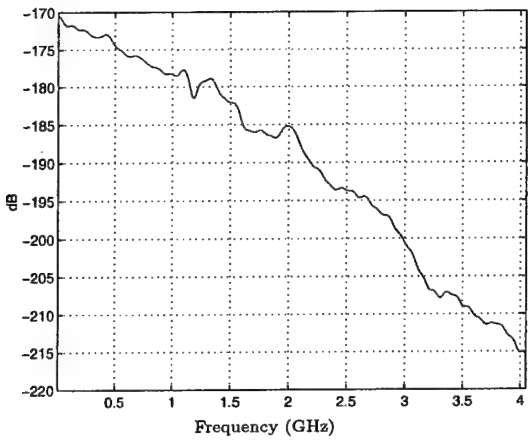

Fig. 7. Spectral density of the template pulse $p(t)$.

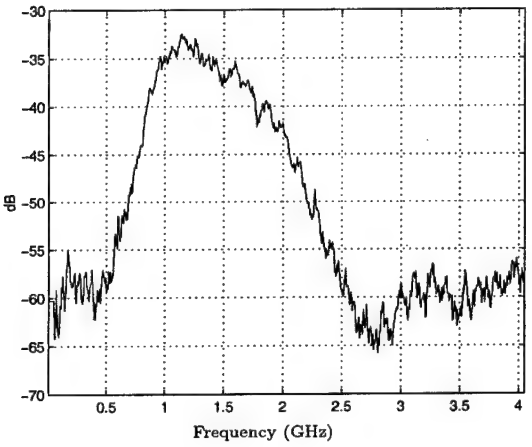

Fig. 8. Measured antenna system function $|H_a(f)|^2$.

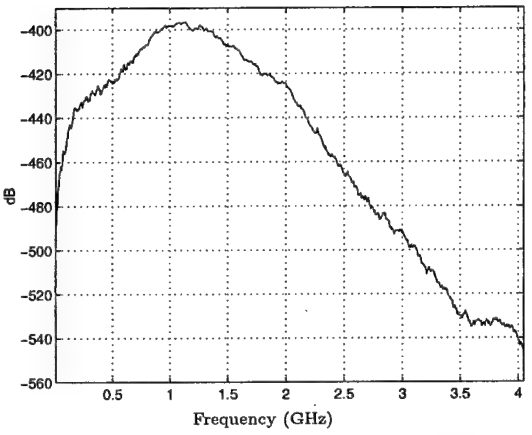

Fig. 9. Plot of $S'_w(f)$ which is evaluated by (28).

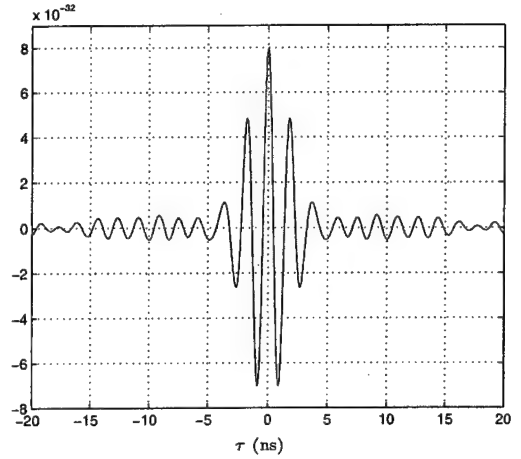

Fig. 10. Plots of the auto-correlation function $R'_w(\tau)$.

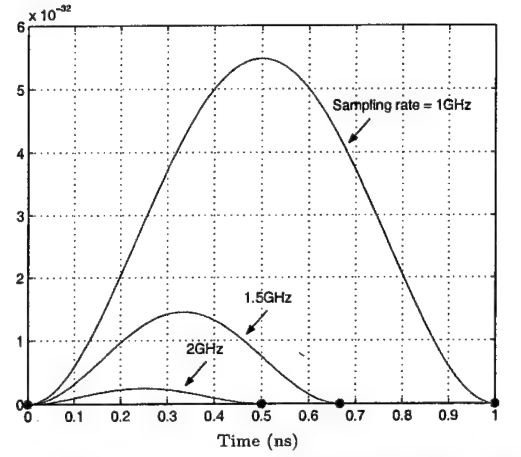

Fig. 11. Evaluation of error variance in MMSE estimation based on 2 samples. Error variance decreases with sampling rate.

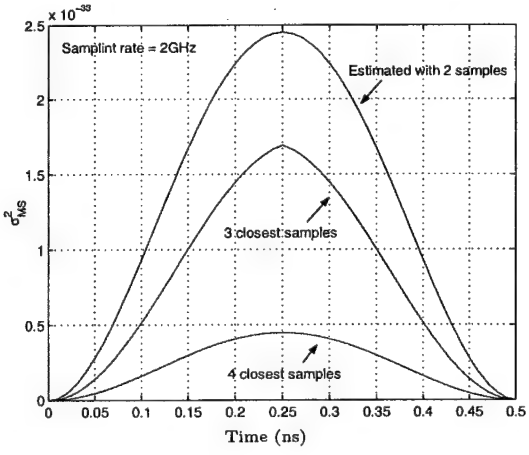

Fig. 12. Evaluation of error variance in MMSE estimation based on different number of samples. Sampling rate was fixed at 2GHz and it was assumed that estimation was done with given number of closest samples.

correlation time of the signal is limited due to the potential clock instability. The sparse-sampling estimation error estimates introduced in this paper can be used to design a fast direct path search in a limited measurement time. To evaluate the error variance of MMSE estimation, a reasonable estimation of the total signal power is necessary.

V. Acknowledgements

The authors would like to thank Profs. Won Namgoong and Keith Chugg for their suggestions.

References

[1] R. A. Scholtz et al., "UWB radio deployment challenges," in *Proc. Personal, Indoor and Mobile Radio Communications (PIMRC 2000)*, 2000, vol. 1, pp. 620–625.

[2] J. M. Cramer, R. A. Scholtz, and M. Z. Win, "Evaluation of an ultra-wideband propagation channel," *IEEE Transactions on Antennas and Propagation*, vol. 50, no. 5, pp. 561–570, May 2002.

[3] M. Z. Win and R. A. Scholtz, "Energy capture vs. correlator resources in ultra-wide bandwidth indoor wireless communications channels," in *Proc. Milcom '97*, Nov 1997.

[4] Joon-Yong Lee and Robert A. Scholtz, "Ranging in dense multipath environments using an uwb radio link," *IEEE Journal on Selected Areas in Communications*, 2002, To be published.

[5] Merrill I. Skolnik, *Radar Handbook*, McGraw-Hill Book Company, New York, 1970.

[6] Malek G. M. Hussain, "Principles of high-resolution radar based on nonsinusoidal waves - part II : Generalized ambiguity function," *IEEE Transactions on Electrmagnetic Compatibility*, vol. 31, no. 4, pp. 369–375, Nov 1989.

[7] Robert J. Marks II, *Introduction to Shannon Sampling And Interpolation Theory*, Springer-Verlag New York Inc., New York, 1991.

UWB Radio Deployment Challenges[1]

R. A. Scholtz, R. Weaver, E. Homier, J. Lee, P. Hilmes, A. Taha, and R. Wilson[2]
University of Southern California, Los Angeles, CA 90089-2565, scholtz@usc.edu

ABSTRACT

The challenges related to the deployment of ultrawideband (UWB) radios are posed in terms of interference issues that UWB radio systems will encounter. The problem of coexistence with a Global Positioning System (GPS) receiver is used as an experimental example. Calculation of an upper bound to UWB transmitter power illustrates the effect of one possible type of regulation for a given UWB antenna system. The inteference environment for a UWB receiver is used to lower bound the UWB transmitter power necessary for a given data rate. Sample measurements are provided.

INTRODUCTION

Ultrawideband radios often are defined to have the property that their 3 dB bandwidth is at least 25% of the center frequency of the radiation. This characteristic means that such radios normally must coexist with many other narrowband signals that occupy their extremely large transmission bandwidth, with none of these systems suffering intolerable interference problems.

The rationale for deploying UWB radio systems lies in the benefits of exceptionally wide bandwidths at the lowest possible frequencies for those bandwidths: (1) very fine time resolution for accurate ranging, imaging, and multipath fading mitigation, and (2) the material penetration capability of relatively low frequencies.

Tolerance of interference to/from coexisting systems comes at a price. The primary objective of this paper is to lay out this problem and give measured examples of the signal environments which may be encountered.

LINK MODELS

A visual model for the interference problem is shown in Fig. 1, which indicates the radiating entities, the receivers of interest, and notation for signals at antenna terminals and useful signals after r.f. processing. The collection of other radiators represents all emitters that radiate power within the bandwidths of the two receivers, including possibly other UWB transmitters, other narrowband systems, etc. Our basic model for the signals present at the outputs of an ultrawideband receiver's antenna and the other

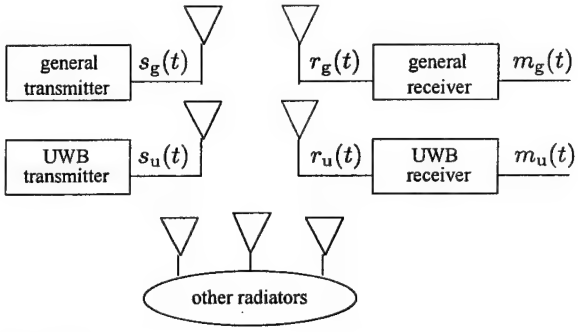

Figure 1: A conceptual block diagram of the interfering signal environment.

general receiver's antenna are denoted by $r_u(t)$ and $r_g(t)$ respectively, where

$$r_u(t) = h_{uu}(t) \star s_u(t) + h_{ug}(t) \star s_g(t) + n_u(t) + i_u(t), \quad (1)$$

$$r_g(t) = h_{gu}(t) \star s_u(t) + h_{gg}(t) \star s_g(t) + n_g(t) + i_g(t), \quad (2)$$

$n_a(t)$ denotes an equivalent receiver noise that represents noise generated within receiver "a", $i_a(t)$ represents the signal induced at the input to receiver "a" by external interference, and the operator $\star$ denotes convolution. For the purposes of these computations, we have represented the transformations from transmitter "a"s antenna input to a receiver "b"s antenna output by a linear time-invatiant transformation with impulse response $h_{ba}(t)$. We further assume that the component signals on the right side of either equation above (e.g., $s_u(t)$, $s_g(t)$, $n_u(t)$, and $i_u(t)$ in the first equation) are wide-sense stationary, mean zero, and uncorrelated with each other.

Although mobility adds another level of complexity to performance calculations and is not considered here, there are no fundamental limitations that would preclude the use of UWB radios in most mobile systems.

Then the power spectral densities of the received signals are given by

$$S_{r_u}(f) = |H_{uu}(f)|^2 S_{s_u}(f) + |H_{ug}(f)|^2 S_{s_g}(f) + N_u + S_{i_u}(f) \quad (3)$$

$$S_{r_g}(f) = |H_{gu}(f)|^2 S_{s_u}(f) + |H_{gg}(f)|^2 S_{s_g}(f) + N_g + S_{i_g}(f), \quad (4)$$

where subscripted $S(f)$ functions represent the corresponding power spectral densities (in watts/Hz), and subscripted $H(f)$ functions represent the system functions (unitless) of the indicated linear time-invariant channels. These system functions are Fourier transforms of the channel impulse responses with the same subscript indicators.

$$H(f) = \mathbb{F}\{h(t)\} = \int_{-\infty}^{\infty} h(t) e^{-j2\pi ft} dt. \quad (5)$$

[1] This work was supported in part by the National Science Foundation under Award No. 9730556, the US Army Research Office through AASERT Grant No. DAAG55-97-1-0245, by the Office of Naval Research through Grant N00014-00-1-0221, and by Compaq through its partnership in the USC Integrated Media Systems Center, an NSF Engineering Research Center.

[2] Dr. Scholtz is Professor of Electrical Engineering. Messrs Hilmes, Homier, Lee, Taha, Weaver, and Wilson are graduate students associated with the Ultra-wideband Radio Laboratory.

As indicated in (3) and (4), the power densities of the equivalent receiver noises are assumed constant and denoted by level N_a in receiver "a".

The receivers of Fig. 1 include those portions of their processing that will improve signal-to-noise ratio, including (a) the rejection of out-of-band signals by filtering, and (b) the achieving of processing gain by spread-spectrum techniques. Let's assume that receiver "a"s desired signal has center frequency f_a, its noise bandwidth is B_a, and its data rate is D_a. We estimate the effective interference power I_a in receiver "a" from other radiators by

$$I_a \approx \int_{f_a - B_a/2}^{f_a + B_a/2} S_{i_a}(f)df \qquad (6)$$

We assume that the power spectral density of the UWB signal at the input to a narrowband general receiver can be approximated by a constant

$$U_g = |H_{gu}(f_g)|^2 S_{s_u}(f_g) \qquad (7)$$

over the operating range of the receiver. We also assume that the desired signal is processed by the receiver without significant distortion and that its total power at the receiver input is denoted by

$$P_a = \int_0^\infty |H_{aa}(f)|^2 S_{s_a}(f)df\,. \qquad (8)$$

Some rough measures of signal quality at the receiver outputs can be calculated from these pieces of information. Specifically the carrier-power-to-noise-power-density ratio at the general receiver can be estimated to be

$$\left(\frac{C}{N_{tot}}\right)_g \approx \frac{P_g}{N_g + U_g + \frac{I_g}{B_g}}, \qquad (9)$$

and the equivalent bit-energy-to-noise-power-density ratio is related to this quantity by

$$\left(\frac{E_b}{N_{tot}}\right)_g = \frac{1}{D_g}\left(\frac{C}{N_{tot}}\right)_g . \qquad (10)$$

Here we have used N_{tot} to represent the effective noise density from all sources including receiver noise and external interference. The effect of interference spectrum spreading in the receiver is embedded in the approximate representation of the interference noise density as flat at the level of the ratio of the interference power to the receiver's noise bandwidth. Similar equations can be written for the corresponding ratios in the UWB receiver.

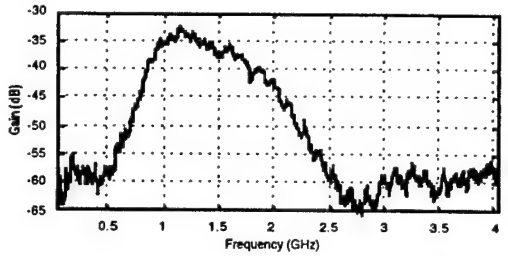

Figure 2: An average of 32 traces of $|H_{uu}(f)|^2$ from the input terminals of a typical small UWB antenna to the output terminals of an identical antenna 1 meter away. Both antennas were vertically polarized and had identical dipole-like antenna patterns. Each antenna was in the maximum-gain direction of the other. The average was taken over measurements in 32 different locations in an indoor environment.

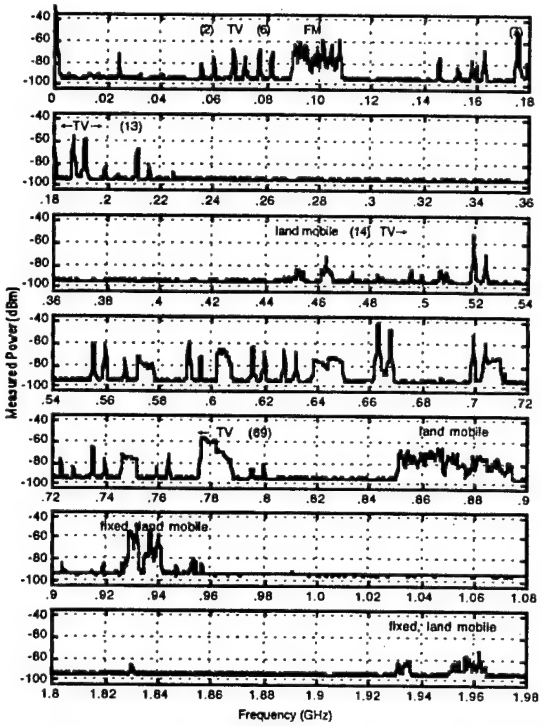

Figure 3: A measurement of interfering signals through one of the UWB antennas of Fig. 2, made in a windowed office on the fifth floor of an office building in Los Angeles. The resolution bandwidth of the spectrum analyzer was set at 300 kHz, and hence the -94.5 dbm measured noise floor corresponds to an equivalent noise power density of -149.3 dBm/Hz. No large interfering signals were measured in the range 1.08 - 1.8 GHz.

INTERFERENCE FROM OTHER RADIATORS

The general and UWB receivers operate under significantly different interference environments, not only because they are not co-located, but also because the general receiver is assumed to be operating in a dedicated frequency band, while the UWB receiver must contend with a potentially large number of narrowband radiators within its bandwidth. The external interference to the UWB receiver is strongly antenna dependent.

Example: Fig. 2 illustrates the measured system function of one possible UWB antenna system (from transmit to receive). Figure 3 shows a crude spectrum analyzer measurement of the interference-only output of one

such UWB antenna in an urban indoor environment. (See [1] for a detailed outdoor radio survey in the Los Angeles area.) It is clear that, at least for this antenna design and environment, a significant amount of lower-frequency interference power (TV, FM, and land mobile radiators) comes through the antenna's frequency sidelobes below the main passband of the UWB antenna system. Hence without any band-limiting filters in the front end of the UWB receiver, the interference power received by an antenna of Fig. 2 in the interference environment of Fig. 3 can be conservatively estimated to be

$$I_{\mathrm{u}} = -33.5\,\mathrm{dBm} \qquad \text{(no bandlimiting)}. \tag{11}$$

This level of interference can be reduced by bandpass filtering in the front end of the UWB receiver.

Reducing the available antenna system bandwidth of Fig. 2 by filtering to the frequency range (780 MHz, 2.05 GHz) eliminates much of the interference power, while utilizing almost 97% of the antenna system's noise bandwidth.

$$I_{\mathrm{u},97\%} = -40.9\,\mathrm{dBm} \quad \text{(97\% bandwidth usage)}. \tag{12}$$

If filtering bandwidth is reduced further to (960MHz, 1.93GHz) to eliminate the strong interferers near its band edges, the interference power in this example is bounded by the noise floor of the spectrum analyzer,

$$I_{\mathrm{u},86\%} < -60\,\mathrm{dBm} \quad \text{(86\% bandwidth usage)}. \tag{13}$$

The progression from (11) to (13) symbolizes the trading of small amounts of the UWB signal's bandwidth (and possibly power) for relatively large reductions in the interference levels in the UWB receiver. Tunable notch filters may be necessary to eliminate the worst narrowband interferers and further reduce I_{u}.

Certainly the interference power I_{u} is a critical and highly variable parameter in determining the UWB transmitter power that is required for proper operation of the UWB receiver. Let $(E_{\mathrm{b}}/N_{\mathrm{tot}})_{\mathrm{u,min}}$ denote the minimum operating bit signal-to-noise ratio that gives satisfactory performance in the UWB receiver. Then, using equations analogous to (9) and (10) for the UWB receiver and assuming that the interference U_{g} from the general system has been included in the measurement of I_{u}, one can show that satisfactory operation is achieved when the received energy per bit $P_{\mathrm{u}}/D_{\mathrm{u}}$ satisfies

$$P_{\mathrm{u}}/D_{\mathrm{u}} > \left[N_{\mathrm{u}} + \frac{I_{\mathrm{u}}}{B_{\mathrm{u}}}\right](E_{\mathrm{b}}/N_{\mathrm{tot}})_{\mathrm{u,min}}. \tag{14}$$

It is worth noting that if I_{u} is dominated by a few strong narrowband interferers, then I_{u} may be highly sensitive to the location of its measurement, the interference suffering from multipath enhancement/fading.

The bound (14) on received signal power P_{u} can be converted to a bound on the transmitted signal power $\overline{P}_{\mathrm{u}}$ for any given channel. Assuming that the transmitted power density is nearly constant over the passband $(f_{\min}, f_{\max})$ of the UWB antenna system, this bound is simply

$$\begin{aligned} P_{\mathrm{u}} &= \int_{f_{\min}}^{f_{\max}} |H_{\mathrm{uu}}(f)|^2 S_{s_{\mathrm{u}}}(f)df \\ &\approx B_{\mathrm{u}} S_{s_{\mathrm{u}}}(f_{\mathrm{u}}) G_{\mathrm{uu}}(R) \approx \overline{P}_{\mathrm{u}} G_{\mathrm{uu}}(R), \end{aligned} \tag{15}$$

where the avarage power gain of the UWB channel is given by

$$G_{\mathrm{uu}}(R) \stackrel{\mathrm{def}}{=} B_{\mathrm{u}}^{-1} \int_{f_{\min}}^{f_{\max}} |H_{\mathrm{uu}}(f)|^2 df. \tag{16}$$

Here we have indicated explicitly the dependence of the channel gain on the range R between the UWB transmitter and receiver, this relationship being embedded in $H_{\mathrm{uu}}(f)$.

UWB INTERFERENCE TO OTHER SYSTEMS

The Federal Communications Commission (FCC) regulates the maximum interference to which a radio system can be subject by an out-of-band interferer. Currently the FCC has no regulation in place which will allow the deployment of commercial UWB products, but proposed regulations are expected to be announced in the near future [2].

Regulations are posed as a function of the electric field strength at a prescribed distance from the transmitting antenna. For two polarization-aligned identical antennas a distance R apart, matched for maximum power transfer to their associated circuits, there is evidence that one can model the transfer function $H_{\mathrm{uu}}(f)$ from one pair of antenna terminals to the other by [3]

$$H_{\mathrm{uu}}(f) = \frac{(j2\pi f)\eta_0}{2\pi c R Z_0} e^{-j2\pi f r/c} [H_{\mathrm{R}}(f)]^2 \tag{17}$$

where $H_{\mathrm{R}}(f)$ is the receiving transfer function[3] (in units of meters) from the electric field reference point near the receiving antenna to the antenna terminals, Z_0 corresponds to the identical source and load impedances, and $\eta_0 = 377\Omega$ is the intrinsic impedance of free space. The $j2\pi f$ in (17) represents a differentiation that is present in the radiation process. We will make use of the power relationships that this equation embodies.

The transfer function $H_{\mathrm{Eu}}(f)$ from the terminals of the transmitting antenna to the electric field at the reference point of the receiving antenna is

$$H_{\mathrm{Eu}}(f) = \frac{H_{\mathrm{uu}}(f)}{H_{\mathrm{R}}(f)}. \tag{18}$$

The transfer function $H_{\mathrm{uu}}(f)$ can be measured by a network analyzer, and hence $H_{\mathrm{R}}(f)$ can be calculated from (17) and $H_{\mathrm{Eu}}(f)$ from (18). The transfer function $H_{\mathrm{Eu}}(f)$

[3] The power gain of the UWB antenna in the direction in which $H_{\mathrm{R}}(f)$ is measured and at frequency f and wavelength λ is given by $|H_{\mathrm{R}}(f)|^2 \times \frac{4\pi}{\lambda^2} \times \frac{\eta_0}{Z_0}$.

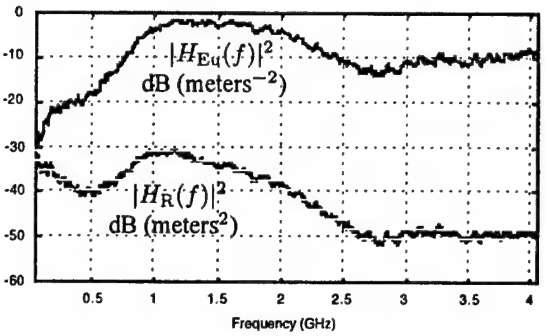

Figure 4: A decomposition of the function $|H_{uu}(f)|^2$ of the antenna system of Fig. 2 into its component functions.

(in units of meters^{-1}) is a key component of electric field calculations for regulatory purposes.

One possible form of regulation for UWB radio signals is to specify that the rms electric field strength measured in any bandwidth B_{reg} at a distance R_{reg} be at most E_{reg} volts/meter. This translates into the bound

$$Z_0 \int_{f_0 - B_{reg}/2}^{f_0 + B_{reg}/2} \left[|H_{Eu}(f)|^2 \right]_{R=R_{reg}} S_{s_u}(f) df < E_{reg}^2 \tag{19}$$

for all f_0. Assuming that the integrand above is a smooth function and that the peaks of $H_{Eu}(f)$ and $S_{s_u}(f)$ approximately coincide for efficiency, (19) can be restated as

$$\max_{f_0} S_{s_u}(f_0) < S^*, \tag{20}$$

where

$$S^* \stackrel{\text{def}}{=} \frac{E_{reg}^2}{Z_0 B_{reg} \max\limits_{f_0} \left[|H_{Eu}(f_0)|^2 \right]_{R=R_{reg}}}. \tag{21}$$

The quantity S^* can be interpreted as the effective regulatory bound on the transmitted UWB signal's power spectral density at the frequency which is most efficiently transmitted by the given UWB transmitting antenna.

If the power spectral density bound S^* is observed by the UWB transmitter across the bandwidth B_u of its antenna system, then the transmitted UWB power $\overline{P}_u$ is reasonably bounded by

$$\overline{P}_u < S^* B_u. \tag{22}$$

An Example: Let's suppose that by regulation a UWB transmitter must create an electric field strength E_u that is at most 500 microvolts/meter at 3 meters from the transmitting antenna, in any 1 MHz band.[4] Compliance with this requirement would have to be checked in an anechoic chamber with a calibrated receiving antenna.

[4] Part 15.109 of Section 47 of the *Code of Federal Regulations* indicates that for signals above 960MHz, the unintentional radiated emission limit for all but Class A devices is 500 microvolts/meter at 3 meters. The example's regulation modifies this in three ways: (1) the emission is intentional, (2) here the level of emission is allowed in every 1 MHz band in which the UWB transmitter radiates, and (3) the example's field strength is not limited to frequencies above 960MHz.

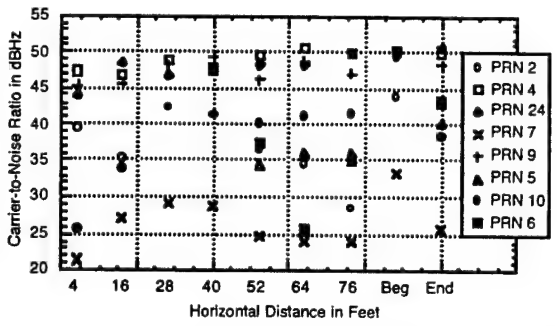

Figure 5: Carrier-to-noise ratios in a GPS receiver for different GPS satellite signals (identified by their PRN codes), as a function of the distance between the fixed GPS receiver and a UWB emitter. The time ordering of the measurements was Beg, 40′, 28′, 16′, 4′, 52′, 64′, 76′, End. The Beg and End measurements were made with the UWB emitter off.

Suppose that a UWB system employing the antenna system of Figs. 2 and 4 must comply with the above requirement. Then the power density bound at 1.15 GHz for the signal being supplied to the transmitting antenna is

$$\begin{aligned} S^* &= \frac{(5 \times 10^{-4})^2}{50 \times 10^6 \times 3^{-2} \times 10^{-.2}} \text{ Watts/Hz} \\ &\approx -131 \text{ dBW/Hz}. \end{aligned} \tag{23}$$

Assuming that this antenna system's bandwidth is roughly 900 MHz, the transmitted power supplied to this antenna would be approximately -12 dBm.

A GPS INTERFERENCE TEST

While FCC regulations are and will be the basis for controls on UWB emitters, it is informative to study the problems that come up in a test of UWB interference to a GPS receiver. Notwithstanding the great variety of GPS antennas and receivers, as well as UWB waveforms, we performed a test in which the UWB antenna of Figs. 2 and 4 was pulsed by a subnanosecond pulse of approximately Gaussian shape (standard deviation parameter = .24 ns) at a rate of a million pulses per second, creating an interference line spectrum with 1 MHz spacing to the GPS receiver. The GPS receiver itself was designed to have a front-end bandwidth of 16 MHz, thereby collecting several of these lines. The results of this interference on the CA code carrier-to-noise ratio $(C/N_{tot})_g$ at the L1 carrier frequency 1.57542 GHz for all satellites in view is shown in Fig. 5.

Certainly it is possible to predict theoretically the observed interference effects based on linear front-end processing in the GPS receiver and knowledge of its noise floor. The experiment described above can approximate the effect of a flat received UWB interference density U_g (see (7)) in the GPS band because there are several spectral lines from the test UWB signal within the RF bandwidth of the GPS receiver. Spread-spectrum processing of the GPS receiver will spread this interference power smoothly over the receiver's correlator output bandwidth, spectrally approximating white noise. The transmitted UWB power is -41 dBW, corresponding to a transmitted power density of ap-

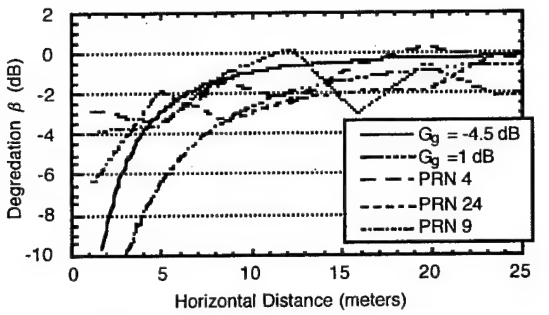

Figure 6: Degredation plots as a function of horizontal distance between the UWB transmitting antenna and the GPS receiving antenna, for the three GPS satellite signals that were stable for the duration of the test.

proximately -76 dBW/MHz in the GPS band, and 5 dB lower than the value of S^* in the example of (23).

Estimating the effect of the GPS receiving antenna on the vertically polarized incident UWB electric field requires taking into account the interaction of this field with the upward looking circularly polarized GPS antenna. (The output terminals of the GPS antenna were not accessible for a network analyzer measurement of the UWB-to-GPS antenna system.) With the UWB antenna at a horizontal distances between 4 and 76 feet from the GPS antenna and roughly 2 feet higher, there are significant axial ratio and linear to circular polarization losses (estimated from specifications) that must be included along with the GPS antenna gain pattern in the calculation of U_g.

When the GPS receiver operates in a linear fashion on the incoming interfering signal, the degredation β in carrier-to-noise ratio $(C/N_{tot})_g$ that is caused by the presence of a UWB signal is computed in terms of changes in the effective noise power density in the GPS receiver, i.e.,

$$\beta = \left(\frac{N_g}{N_g + U_g} \right), \qquad (24)$$

where U_g is given in (7). Using an effective GPS receiver noise temperature of 300°K, the theoretical and experimentally measured values of $(C/N_{tot})_g$ degredation β are shown in Fig. 6. It is assumed that the effects of multiple-access interference from other GPS signals are included in the GPS receiver's noise power density N_g.

There is good agreement in Fig. 6 between measurement and theory for distances beyond 5 meters, but our predictions of degredation at shorter ranges are worse than the measured degredations. While there are many approximations that could partially account for these discrepancies, one conjecture that might explain this difference is that the GPS receiver's processing was driven out of its linear region at short range by the impulsive nature of the UWB pulse interference, reducing the interfering pulse power by clipping the UWB pulses.

In all of these measurements, the GPS receiver always produced a position measurement, i.e., it always could access enough satellite signals to complete a position location estimate. We believe that the selective availability effects

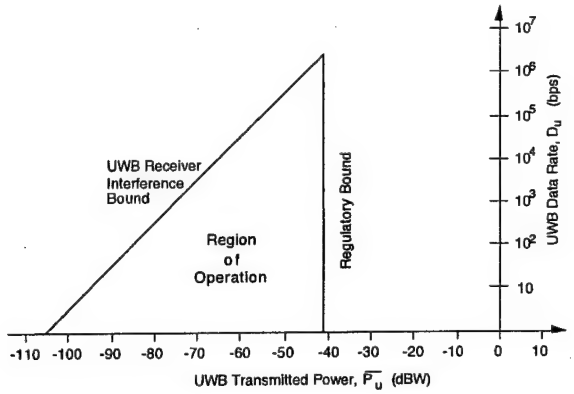

Figure 7: The region of the $(\overline{P}_u, D_u)$ plane representing the operating range of UWB systems. The numerical values used in plotting the bounds on the region of operation come from the examples used in this paper, with numerical values provided by (13) and (23), scaled to an operating range of 30 meters, with $(E_b/N_{tot})_{u,min}$=10 dB.

imposed on the satellite signals for ordinary GPS navigation would completely mask the error effects caused by the UWB interference in these tests. The UWB interference effects may have somewhat more effect on differential GPS systems, but the carrier-to-noise ratio effects are the same in both cases. For experiments with a variety of GPS receivers, but not instrumented for $(C/N_{tot})_g$ measurements, see [4].

UWB SIGNAL POWER BOUNDS

The upper bound on UWB transmitted power $\overline{P}_u$ based on interference to other systems, and the lower bound based on the effects of interference to the UWB receiver are summarized here.

$$S^* B_u > \overline{P}_u > \frac{D_u}{G_{uu}(R)} \left[N_u + \frac{I_u}{B_u} \right] (E_b/N_{tot})_{u,min} \qquad (25)$$

It is worth noting that there is always a critical value of data rate D_u below which the upper bound exceeds the lower bound and communication is feasible in principle.

The deployment challenges for UWB systems are epitomized by the region of operation in in Fig. 7, both in defining that region, and in controlling its boundary to increase the maximum bit rate at which communication will be possible. Clearly, dB changes in the range of allowable transmitter power $\overline{P}_u$ for a given data rate $D_u$translate directly into dB changes in the potentially achievable data rate D_u. There are significant dB uncertainties in these bounds, even for the examples in this paper, because of approximations in the mathematical models used, and uncertainties in the real environment into which a system will be deployed.

The upper bound on the transmitter power can be raised by expanding bandwidth, improving antennas, etc., and is subject to conjecture until the FCC settles regulatory issues.

The lower bound is dominated by interference that may occur in the UWB receiver, and in particular by the quan-

tity I_u/B_u. Since I_u is measured in the operating bandwidth B_u, The system designer should explore the choice of passband to maximize this ratio, within the constraints imposed by propagation effects and hardware constraints.

The boundaries of the operating region have been illustrated here in a relatively simple way. Assumptions have been made in developing these bounds that may be optimistic or pessimistic for a given system and environment. When the bounds on $\overline{P}_u$ are tight and account for the inefficiencies and the realities of an implementation, then the difference between the upper and lower bounds in (24) for a given data rate D_u represents a measure of the achievable link margin for the UWB system. Hence the higher the data rate D_u, the lower the margin available to accomodate unforseen interference and propagation problems. Using the example of Fig. 7 which indicates a critical data rate of roughly 3 Mbps, a margin of 20 dB in the power budget would could be achieved only for data rates below 30 Kbps.

ISSUES IN COMPLETING THE UWB LINK

Communication over paths with a clear line-of-sight can be done in a variety of ways. The potential advantage of UWB radio comes from the ability of low-frequency radio waves to penetrate materials [5]. It is this capability that makes UWB systems competitive with other higher-frequency systems of comparable bandwidth. From another viewpoint, it is the very large bandwidth of a UWB system, which makes it ideal for ranging and provides multipath resolution, that makes it competitive with narrower bandwidth systems within its frequency range.

In many environments, the UWB signal undergoes a significant amount of distortion in the process of propagating from transmitter to receiver. A sub-nanosecond pulse may reverberate in an indoor environment for a few hundred nanoseconds, making complete reception or equalization of the UWB signal difficult. The UWB receiver must track (or compensate for) these distortions to take full advantage of all of the received power for communication purposes. Estimates [6] of the number of resolvable signal components that must be tracked to capture a given percentage of the total incident UWB signal power in an indoor environment can vary significantly over relatively small changes in antenna location because of individual path shadowing, etc. The temporal diversity inherent in such a selective-Rake UWB receiver may be equivalent to a level of directional/ spatial diversity because different components of the received signal arrive at the receiver along spatially distinct paths [7]. These all are considerations in the design of a robust and efficient UWB receiver processing algorithm.

Deployment of UWB radio systems in large numbers with multiple access to the environment can be accomplished by code-division multiple-access techniques. However, accurate prediction of the numbers and possible spatial distribution of UWB radios that may occur in the future is very difficult to estimate or bound. Hence, the aggregate interference that the successful deployment of UWB technology may cause to other systems is not a reliably predictable quantity at the present time. Indeed this concern may lead to regulations that are ultimately too restrictive (or too liberal) in their control of UWB emissions.

ACKNOWLEDGMENT

The authors wish to thank Profs. Keith Chugg, Won Namgoong, and Aluizio Prata for their useful comments and suggestions.

REFERENCES

[1] F. Sanders, B. Ramsey, and V. Lawrence, *Broadband Spectrum Survey at Los Angeles, California,* NTIA Report 97-336, U.S. Department of Commerce, May 1997.
[2] See the Ultrawideband Working Group's web page at http://www.uwb.org.
[3] R. C. Robertson and M. A. Morgan, "Ultra-Wideband Impulse Receiving Antenna Design and Evaluation" in *Ultra-Wideband Electromagnetics 2,* L. Carin and L. B. Felsen, eds., Plenum Press, 1995.
[4] G. R. Aiello and G. D. Rogerson, "Assessing Interference of Ultra-Wideband Transmitters with the Global Positioning System – A Cooperative Study," Institute of Navigation, National Technical Meeting 2000 (available at http://www.fantasma.net/publications.html).
[5] L. M. Frazier, "Radar Surveillance through Solid Materials," SPIE Photonics East Conference, Boston, MA (Paper 2938-20), November, 1996.
[6] M. Z. Win and R. A. Scholtz, "On the Energy Capture of Ultrawide Bandwidth Signals in Dense Multipath Environments," *IEEE Communications Letters,* 2(9), pp. 245-247, Sept. 1998.
[7] See papers available in the library section of the UltRa Lab's web site http://ultra.usc.edu/ulab/.

ULTRA WIDEBAND INTERFERENCE EFFECTS ON AN AMATEUR RADIO RECEIVER

R. D. Wilson, R. D. Weaver, M.-H. Chung and R. A. Scholtz

UltRa Lab
Communication Sciences Institute
University of Southern California

ABSTRACT

This paper illustrates the complexity of issues that arise in the accurate measurement and interpretation of ultra-wideband (UWB) interference effects in narrowband receivers. The behavior of an amateur radio receiver in the presence of sinusoidal and UWB interference is studied. We characterize antenna response and receiver non-linearities, which lead to an understanding of UWB effects on the receiver output during outdoor response measurements as a function of range and antenna orientation.

1. INTRODUCTION

Ultra Wideband (UWB) Radio uses radio impulses to transmit information [1]. The key concept underlying UWB radio is that by using low power spread over a very wide bandwidth, one may communicate information without seriously degrading the performance of other narrowband users in the same frequency range. An important area of research in UWB radio is to quantify the effect that UWB transmissions will have on systems with which spectrum is shared. Radio amateurs are one of the groups concerned with this issue because there are bands allocated for amateur radio within the possible range of future UWB systems. This paper describes the results of sensitivity and linearity measurements performed with a receiver system supplied by the American Radio Relay League (ARRL) to quantify the effects of UWB signals. Testing was performed at the University of Southern California (USC), using the experimental UWB transmitter and instrumentation of USC's UltRa Lab. The receiver and its antenna were supplied by the ARRL, which also provided samples of their standard receiver test procedures.

Sophisticated radio amateurs often use their receiving equipment near the limits of its sensitivity in both practical and experimental settings. The Minimum Discernible Signal (MDS) test was suggested by the ARRL [2] as a measure of how strong a desired signal must be in order to be detected. The MDS paradigm provides a useful framework within which to think about the interference problem, in a particular setting. However, one would like to say something more general, namely how much UWB interference will be detected under a range of conditions (UWB source power, range and propagation geometry). This requires a propagation model and an understanding of receiver non-linearities. Early on in our testing, it became clear that we would need to put particular emphasis on characterizing the non-linearities, because our UWB signal was pulsed with high peak-to-average power ratio, and the receiver had quite narrow dynamic range.

This work was supported in part by the National Science Foundation under Award No. 9730556, by the Office of Naval Research through Grant N00014-00-1-0221, by the MURI Project under Contract DAAD19-01-1-0477, and by the Integrated Media Systems Center, an NSF Research Engineering Research Center.

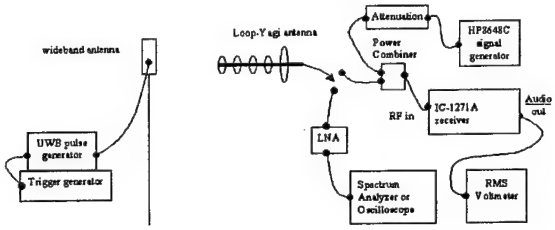

Fig. 1. Experimental setup

2. TESTING PROCEDURES

The test setup is shown in Figure 1. Tests were performed using the UltRa Lab's UWB transmitting equipment, namely a custom-built time hopping trigger generator, an Avtech gaussian pulse generator and a wideband omnidirectional antenna. A variable attenuator was used for power control. The ARRL provided an ICOM IC-1271A receiver and a loop-Yagi antenna as a typical amateur radio setup on which to investigate the interference effects. Details on the UWB signal and antenna characteristics are given in Section 3.

The receiver was operated in the upper-sideband mode, with all other signal processing options, including auto-

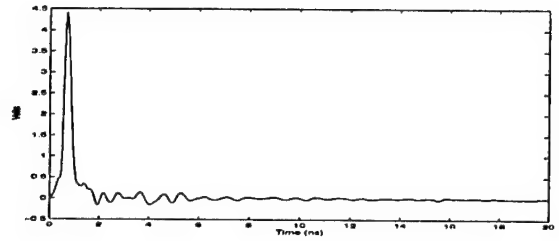

(a) Pulse shape at the pulser output

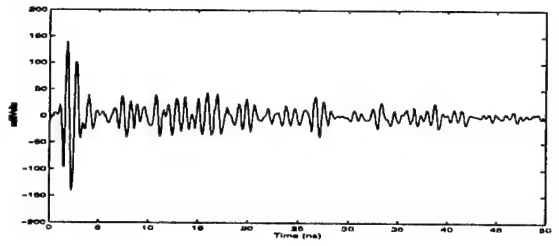

(b) Waveform received by a UWB antenna

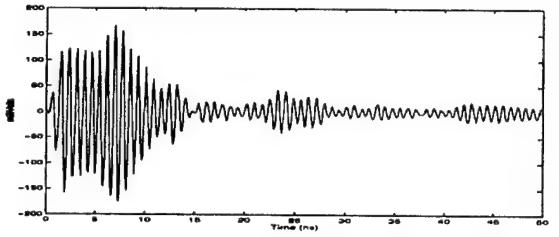

(c) Waveform received by the loop-Yagi antenna

Fig. 2. UWB waveforms

matic gain control, turned off. The RF gain was set at maximum while the audio gain (volume) knob was adjusted so that audio noise output was nominally 30 mV(RMS) when no input was present. The audio "tone" control was set to mid-range. A digital voltmeter was used to measure the audio output.

Testing included signal characterization and linearity tests in a laboratory environment, followed by interference measurements outdoors.

UWB signal characterization was done with a HP54750A high-speed oscilloscope and a HP8563E spectrum analyzer. Since neither instrument has particularly good noise figure, a broadband low-noise amplifier (LNA) was inserted where needed to aid in these characterizations. All measurements are corrected for the gain of

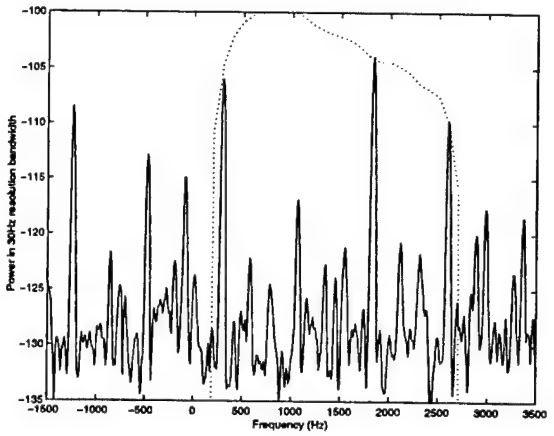

Fig. 3. Narrowband spectrum analyzer trace of the received UWB signal at full power, overlaid with the receiver's audio passband when tuned to 1296 MHz (dotted line, with arbitrary dB offset). The resolution bandwidth is 30 Hz.

the LNA and for cable losses, where applicable.

To evaluate receiver linearity, the output of the receiver tuned to 1296 MHz was observed over a range of radiated UWB powers, to determine what level of UWB interference will drive the receiver into saturation. As a basis for comparison, the same test was performed using a calibrated continuous wave (CW) input to the receiver, such as to produce a 1000 Hz audio tone.

The MDS is the input signal level required to cause a 3 dB rise in the output audio power with respect to the power when no input is applied. If the receiver is operating linearly, it is a measure of the input noise-plus-interference power within the passband of the receiver. Therefore, measuring the output power of the receiver, in linear response conditions, also yields the MDS if the receiver gain is known.

3. SIGNAL AND ANTENNA CHARACTERISTICS

The elementary UWB signal used in these tests is a gaussian pulse of approximately 0.7 ns duration at 50% amplitude and with 90% bandwidth of 1.5 GHz. The pulse shapes at the output of the pulser, after transmission between two ultra-wideband diamond-dipole [5] antennas, and after transmission between one diamond dipole and the loop-Yagi are shown in Figures 2(a), (b) and (c), respectively.

The time-average pulser output power is -10.3 dBm in the time-hopped mode, including transmission line losses between the pulser and transmit antenna. The time hopping system generates a sequence of 1023 pulses, randomly pulse position modulated at an average interval of 1.27μs,

thus producing an overall waveform period of 1.3 ms. In Figure 3, the UWB spectrum is shown over a 4 kHz range about 1296 MHz, measured between a wideband diamond-dipole transmit antenna and the loop-Yagi receive antenna at a separation of 3 m. Overlayed is the measured frequency response of the ICOM receiver when tuned to that frequency, plotted on an arbitrary dB scale.

Because of its periodicity, the UWB test signal has a line spectrum. The 1.3 ms period indicates that we should expect spectral lines at intervals of approximately 770 Hz. The expected 770 Hz spaced lines are apparent, as are other, generally weaker, lines due to idiosyncracies of the transmitter hardware. All measurements were performed using no data modulation. Random data modulation will disrupt the periodicity of the signal and therefore further smooth the distribution of power over frequency.

The UWB antenna gain pattern and frequency response are plotted in Figure 7(a). Its polarization is vertical. The gain pattern and frequency response of the loop-Yagi antenna are shown in Figure 7(b). Its polarization was found to be nearly linear and it was oriented for maximum response. To ensure repeatable results, the loop-Yagi was pointed directly at the UWB antenna during signal characterization and linearity testing.

4. EXPERIMENTAL RESULTS

In Figure 3, we can see how the UWB spectrum relates to the passband of the receiver tuned to 1296 MHz. There are four major spectral peaks within the receiver passband. As the receiver is tuned, a different number of peaks may enter the band and the detected interference power may change. Because the receiver passband is approximately 2.5 kHz, and the peaks are spaced at 770 Hz intervals, there will always be three or four peaks within the passband, so we should expect a variation in interference level of about 4/3 or 1.25 dB, plus any variations due to the shape of the signal spectrum itself. We will see in section 4.2 that the interference level varies about 3.5 dB when receiver response is linear.

4.1. Receiver Linearity

The receiver linearity was characterized for both UWB and sinusoidal signals. In Figure 4 we see that the receiver behaves differently in each case. The response due to the calibrated CW source may be considered as firmly known, while the horizontal alignment of the UWB curve was more difficult to establish. It involves estimating the portion of input power, already filtered by the antennas, contained within the passband of the receiver. This may be done by reference to Figure 3, or using the time domain waveform of Figure 2(c). In the latter case, we can estimate the average

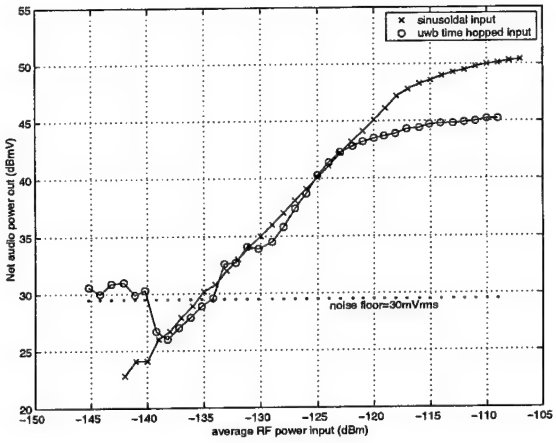

Fig. 4. Receiver linearity at maximum RF gain. Antenna separation was 2 m for the UWB case.

power in the passband of the receiver by taking a discrete Fourier transform and using our knowledge of the average pulse period. By this method, at full transmitter power (the rightmost point in Figure 4), the average received UWB power within the receiver passband is approximately -107 dBm, which justifies the horizontal positioning of the UWB curve to within 2 dB.

Assuming that our placement of the UWB curve is correct, the plot shows that the receiver begins to behave non-linearly at approximately 5 dB lower average input power when the UWB signal is present compared to the sinusoidal signal. Also note the 5 dB lower compressed output level for the UWB signal. This is thought to be due to the low duty cycle of the pulse waveform, in that the receiver is in compression due to the high peak power, but this amount of power is not always present as it would be in a sinusoidal signal. For some portion of the time between pulse arrivals the input power is much lower than the peak and the receiver is not saturated, therefore although the response is non-linear, the average output power is reduced.

The 5 dB difference in both the compressed output power and the saturation point suggests a duty cycle for the UWB waveform within the receiver of approximately 30% at the point where compression occurs. This indicates that the pulses are undergoing compression in an early IF stage with bandwidth of about 2.5 MHz. With the receiver in compression, the measured interference level is lower than would be the case if response were linear. The compressed receiver stage acts as a bandpass limiter, which is well known to help reduce the effects of pulsed interference. A lower duty cycle UWB signal of equal average power, whose higher peak power would be compressed in an earlier receiver stage, would produce even less output interference.

The UWB linearity plot shows that the receiver will op-

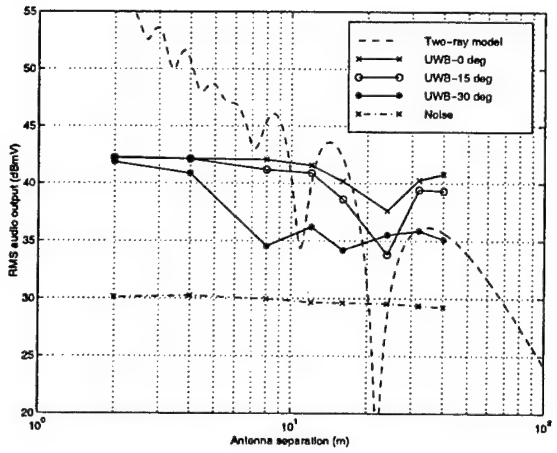

Fig. 5. Measured audio output vs. range and antenna boresight angle. An idealized two-ray model is shown for comparison.

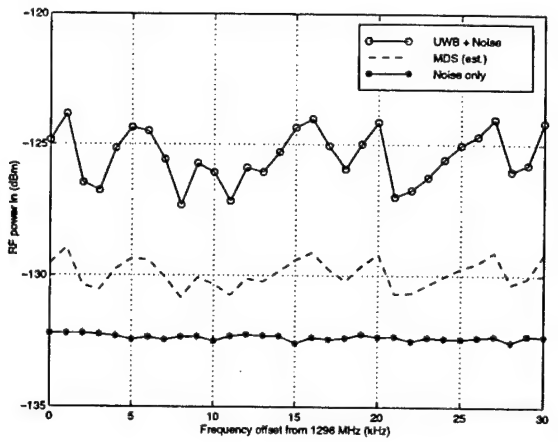

Fig. 6. Outdoor UWB response measured at 24 m range and 30 degrees off boresight. The MDS estimate is corrected for the excess power of our transmitter.

erate linearly if the input power is reduced by at least 15 dB. Therefore, increasing antenna separation to a minimum of approximately 12 meters in free space should also result in linear operation. This estimate of minimum separation is supported in the following section.

4.2. Outdoor Measurements and MDS Estimate

Outdoor tests were performed to confirm ranges and antenna orientations where the receiver could be expected to behave linearly. This was done on the top floor of a parking structure at USC. In addition to the direct path and the ground reflection, there may have been other significant reflections due to perimeter walls and metal fences. The audio output of the receiver was measured at different separations and the receiving loop-Yagi antenna was pointed 0, 15 and 30 degrees away from the transmit antenna, with the UWB signal at full power. The results are shown in Figure 5. Here, measured noise is subtracted from the UWB measurements.

Also plotted are the predictions of a simple two-ray model over an ideal ground plane, modified from [3]. The model assumes idealized antenna patterns similar to Figure 7 and linear response extrapolated from Figure 4. Clearly the model does not match the measurements very well, but it does provide a useful frame of reference in which to interpret our results. Viewed in this light, the data support our expectation that audio output is compressed to a constant for separations less than about 12 meters with the loop-Yagi antenna boresighted, due to the non-linearity of the receiver. The presence of a shallow null near 20 meters also suggests that we are on the right track, but that the reflected ray is considerably weaker than is assumed by the model.

Having determined the minimum antenna separation required by the receiver to operate linearly, we performed a final series of measurements aimed at estimating the MDS. We chose a 24 meter separation, with the receiving loop-Yagi antenna pointed 30 degrees away from the UWB transmitter. The test was done over a 30 kHz span in 1 kHz steps beginning at 1296 MHz, with the UWB signal alternately turned on and off. The results are shown in Figure 6. The scaling of the vertical axis is based on Figure 4. The UWB signal produced an output power 5 to 8 dB above the receiver noise floor, while the noise varied less than 1 dB. The variability of the UWB-induced output is due to the line spectrum of the UWB signal.

5. COEXISTENCE AND REGULATION

In this paper, we studied the behavior of an amateur radio receiver in the presence of the UWB interference. It is important to understand the limitations of the data presented above.

Our UWB signals did not conform to proposed UWB regulatory limits on average power spectral density [6]. The limit, below 2 GHz, is 12 dB below 500 μV/m into any 1 MHz of bandwidth at 3 m. Our calculations show that our output at 1296 MHz was 287 μV/m per MHz, or roughly 7 dB higher. Figure 6 shows our best estimate of what the receiver's MDS might have been if our transmitter had been in compliance with the proposed limit.

Test configurations were chosen, not as realistic interference scenarios, but rather to facilitate obtaining reasonably clean and repeatable measurements and to achieve an

understanding of potentially important effects. Pointing a beam antenna directly at the source of UWB interference at close range in an enclosed space, as we did, is a good way to measure interference effects, but the results cannot be taken as a direct illustration of the impact of UWB on amateur radio in general.

Despite our emphasis in this paper on characterizing and later avoiding non-linearities in receiver response measurements, one should not assume that this non-linear behavior is undesirable. To the contrary, in this case, a high peak-to-average power ratio UWB signal caused less interference than did a CW input having equal average power in-band, as was pointed out in Section 4.1. Notwithstanding any other considerations motivating FCC's proposed limits on peak-to-average power ratios, this narrowband receiver system would probably benefit from an even higher ratio. Since the pulse width seen by the receiver is effectively set by its antenna, this might mean raising the UWB pulse amplitude while slowing the pulse repetition frequency to maintain the same average power level.

Acknowledgments

The authors wish to thank ARRL, and particularly Ed Hare for the use of their receiver. Thanks are also due to S. Chang, C.-C. Chui, M. Nemati, S. Ramanujam and R. Tarif for their help with the experiments.

6. REFERENCES

[1] R. A. Scholtz and M. Z. Win, "Impulse Radio," invited paper, *Proc. PIMRC'97*, Sep 1997.

[2] M. Tracy and M. Gruber, *Test Procedures Manual, Rev. F*, American Radio Relay League, June 2000.

[3] T. S. Rappaport, *Wireless Communications: Principles & Practice*, Prentice Hall, 1996.

[4] R. A. Scholtz et. al., "UWB Deployment Challenges," invited paper, *Proc. PIMRC'00*, Sep. 2000.

[5] H. G. Schantz and L. Fullerton, "The Diamond Dipole: A Gaussian Impulse Antenna," *Proc. IEEE AP-S Int. Symp.*, July 2001.

[6] Federal Communications Commission, "Revision of Part 15 of the Commission's Rules Regarding Ultra-Wideband Transmission Systems," *NPRM 00-163*, May 10, 2000.

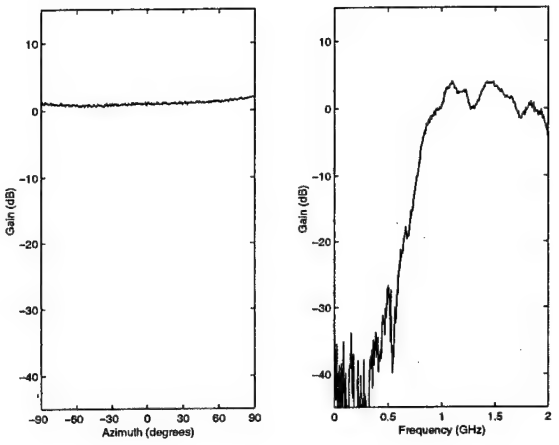

(a) UWB antenna

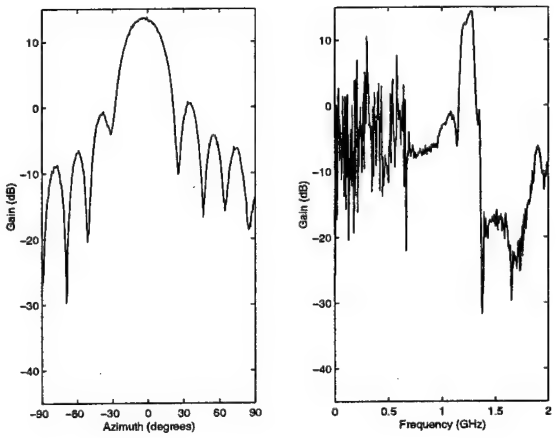

(b) 14-element loop-Yagi antenna

Fig. 7. The 1296 MHz azimuth pattern and boresight frequency response of the two antennas

Technical Report

Naval Total Asset Visibility (NTAV) Tests on the SS Curtiss, Port Hueneme, CA 25 September – 6 October 2000

Appendix A
USC UltRa Lab: Shipboard Environment Characterization

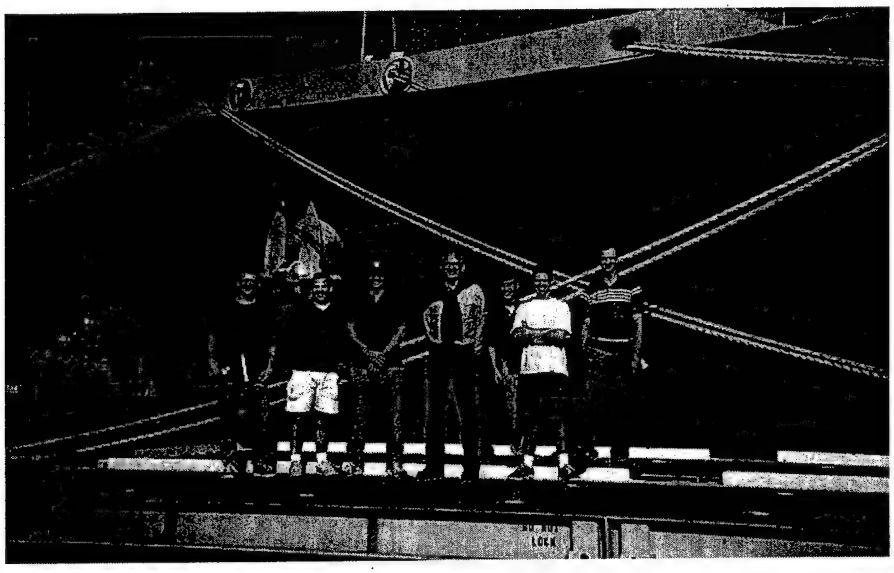

March 2002

Naval Facilities Engineering Service Center

Steven J. Gunderson

University of Southern California

Dr. Robert Scholtz
Dr. Keith Chugg
Mr. Robert Weaver
Mr. Joon-Yong Lee
Mr. Carlos Corrada
Mr. Eric Homier
Mr. Robert Wilson

The University of Southern California (USC) Ultra Lab conducted shipboard RF environment characterization of the SS Curtiss immediately following the first week open space tests. Tests were not performed during the second week with containers. Dr. Robert Scholtz led the team of professors and students. The test provided an excellent opportunity for USC to perform channel measurements in a ship. They were funded by ONR Code 313 Marine Corps 6.1 research grant.

Four primary tests were run:

- Pulse Response with Sampling Oscilloscope
- Transfer Function with Network Analyzer
- Pulse Response with a UWB Test Radio
- Interference Check with Spectrum Analyzer

The pulse response with sampling scope test was straightforward, operating similar to container tests conducted by AetherWire at the Port of Oakland. A low-powered pulser was connected to an UWB "diamond" antenna to radiate impulses. Synch reference was provided by coax cable to the sampling oscilloscope. Measurements were made with a 20 Gsample/sec sampling oscilloscope connected to a pre-amplifier and matching "diamond" antenna. Figure A-1 shows the pulse generator and oscilloscope equipment configuration.

The sampling scope had limited memory, thus many readings needed to be spliced together to form a composite picture, lengthening time required for measurement and limiting the number of tests that could be made. The sampling oscilloscope had high background noise, limiting noise floor, preventing measurement to –20 dB. Averaging was not used due to the long measurement times.

The network analyzer was used to improve noise floor. It measured the channel frequency and phase response and the result was Fourier transformed into the time domain. It had 40 to 50 dB lower noise floor than the digital sampling oscilloscope. Ship's high pressure sodium arc lamps were turned off, as they raised the noise floor 6 dB. Figure A-2 shows the network analyzer test equipment configuration.

The UWB test radios were Time Domain PulsON™ Application Demonstrator (PAD). They operated in pairs, one transmitting and the other receiving. They were used for channel measurements and sampled the environmental response, much the same as a pulse generator/sampling oscilloscope. They did not need a synchronization cable between units, they were able to automatically synchronize between themselves from received pulses. Samples were sent to a connected laptop PC. No pictures were taken of the PADs and no data was made available. Time domain provided the units to USC non-disclosure.

A spectrum analyzer was used to measure interference from shipboard radios and radars.

UWB "diamond" antennas were used for all tests. They are like "bow-tie" antennas, with broad response, but have the "fat" side connected inside resulting in a diamond appearance. The PADs have smaller "diamond" antennas, and the oscilloscope and network analyzer measurements used larger antennas with –3 dB response from 700 MHz to 1.8 GHz. Figures A-3 and A-4 show a test setup in holds 5 and 6. Figures A-5 thru A-7 show the measurement equipment, measurements and data processing equipment.

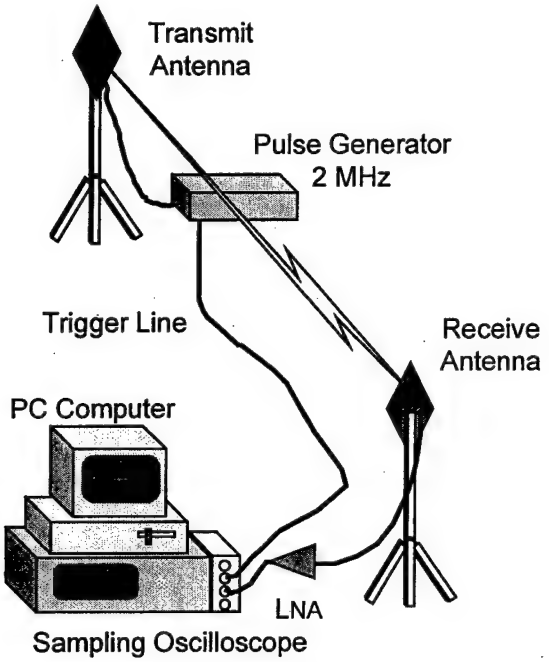

Figure A-1. USC pulse generator and sampling oscilloscope test equipment.

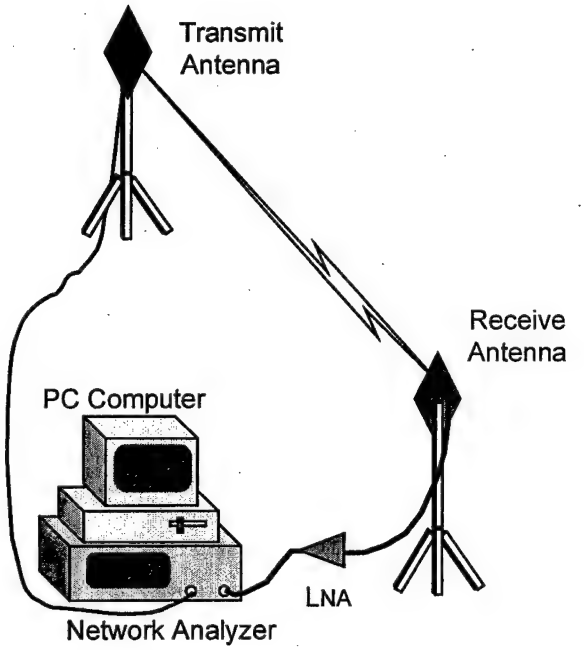

Figure A-2. USC network analyzer test equipment.

Figure A-3. USC test equipment setup in SS Curtiss Holds 5 and 6, looking port forward.

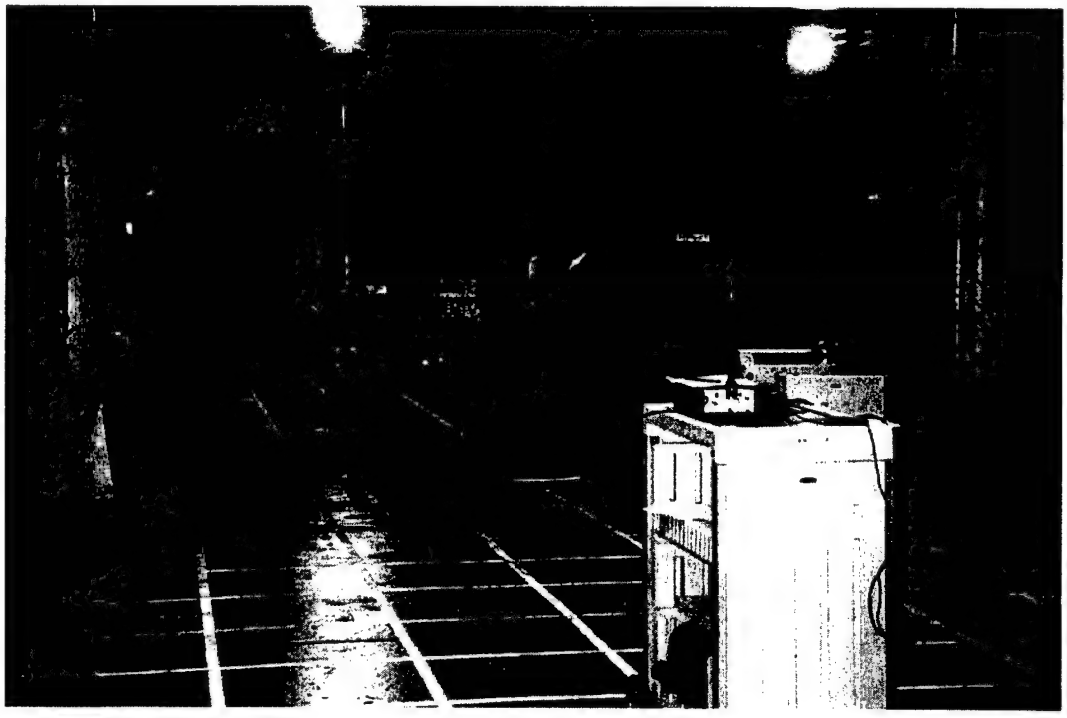

Figure A-4. USC test equipment setup in SS Curtiss Holds 5 and 6, looking forward.

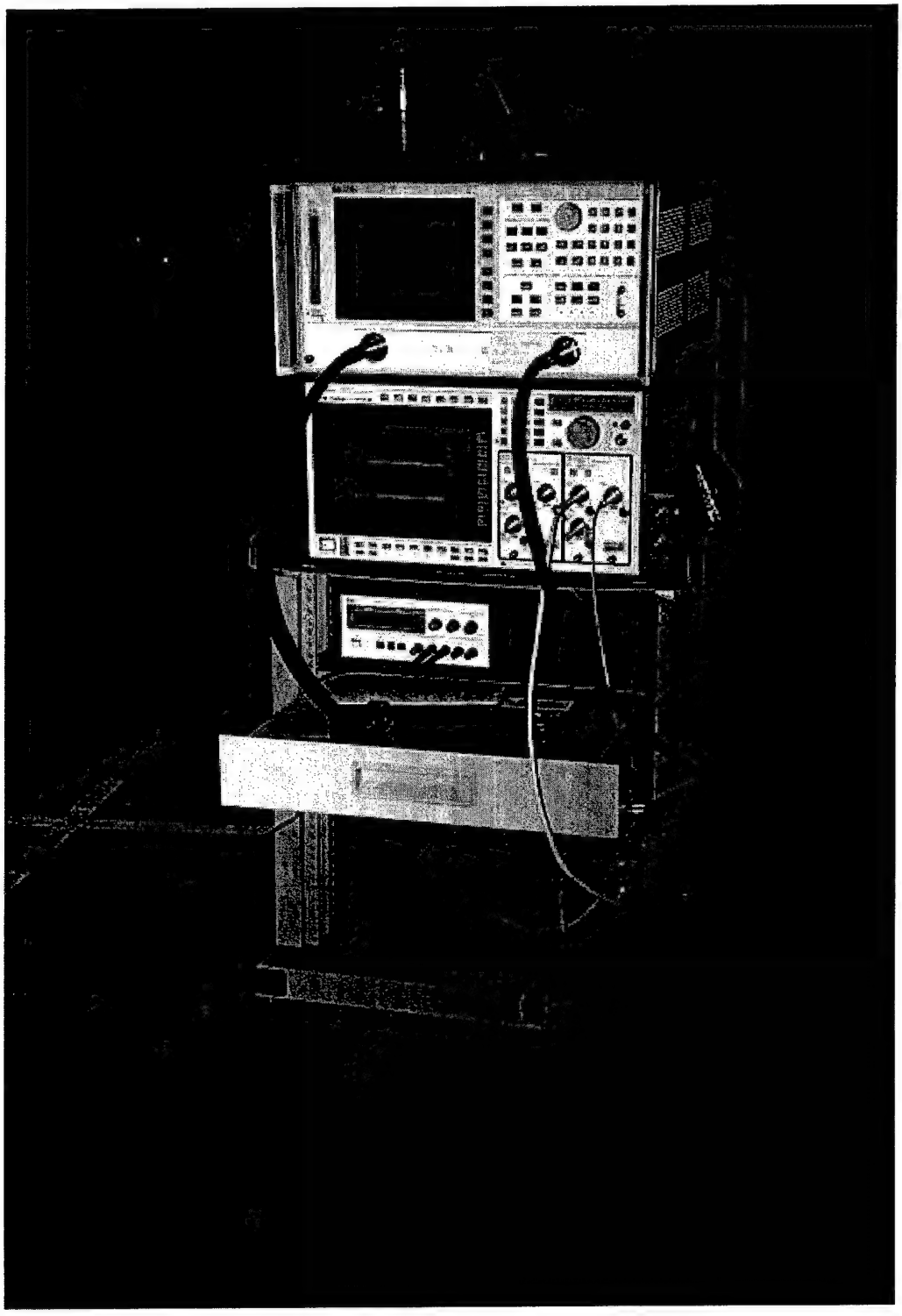

Figure A-5. USC network analyzer and sampling oscilloscope.

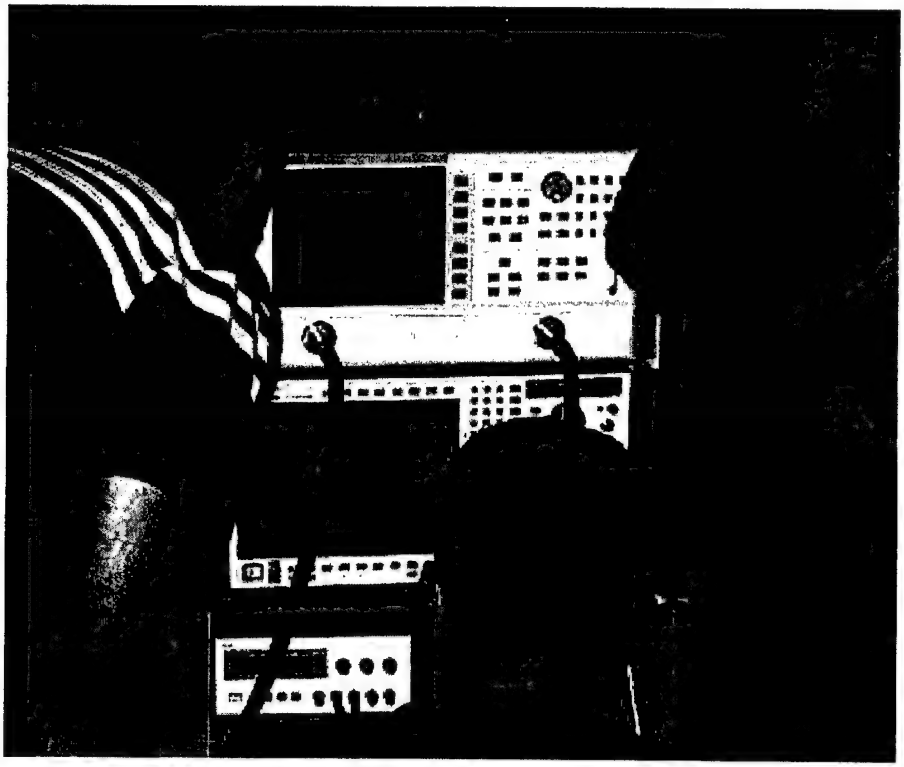

Figure A-6. USC team taking measurements.

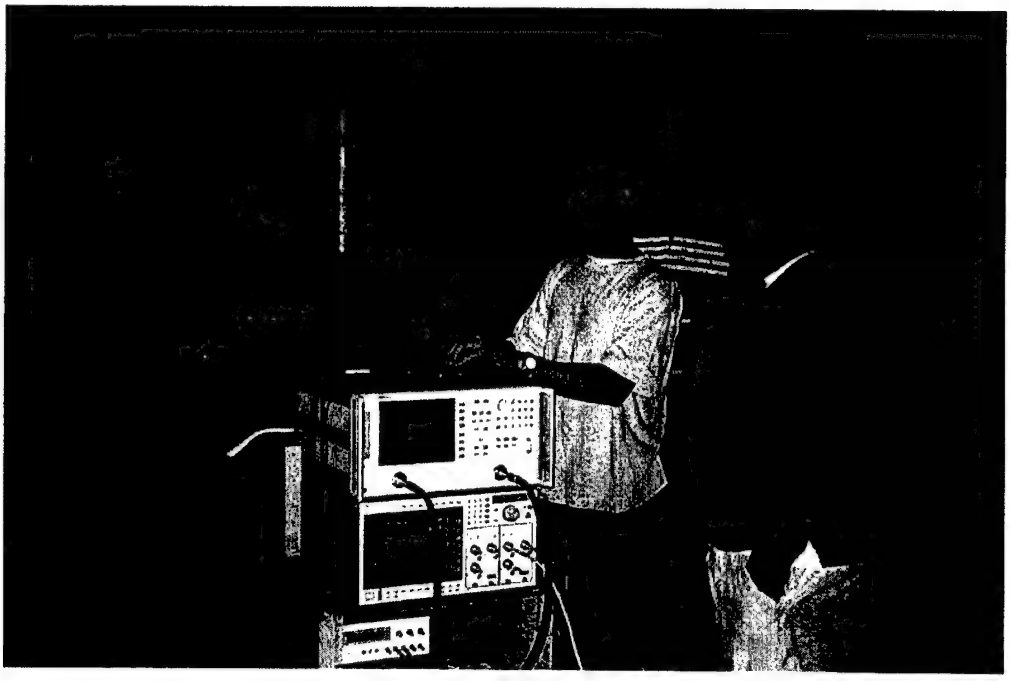

Figure A-7. USC team processing measurements with PC and MATLAB.

Five different channel measurement tests were made with antennas in different locations, each with sampling oscilloscope and network analyzer. Figures A-8 through A-12 show the test configurations. The transmit antenna is the triangle and the receive antenna is the circle.

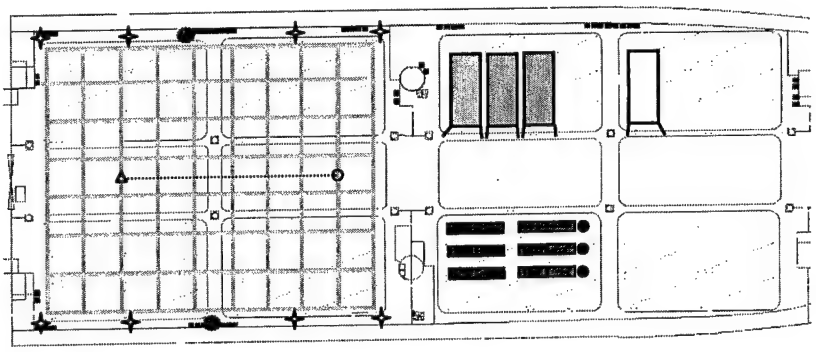

Figure A-8. Test 1 Configuration – 60-foot distance, down the middle.

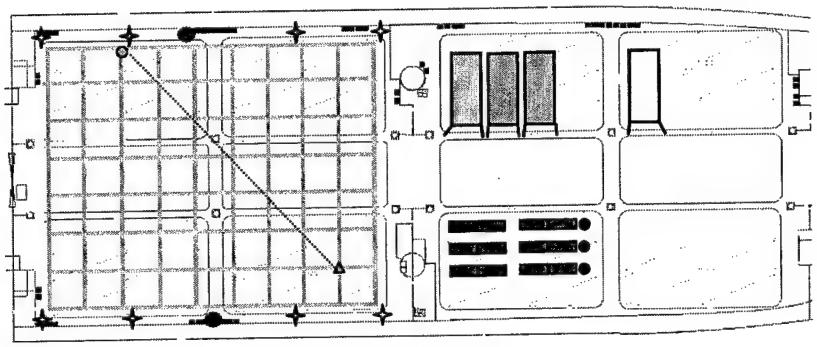

Figure A-9. Test 2 Configuration – 85-foot Distance, through a stanchion.

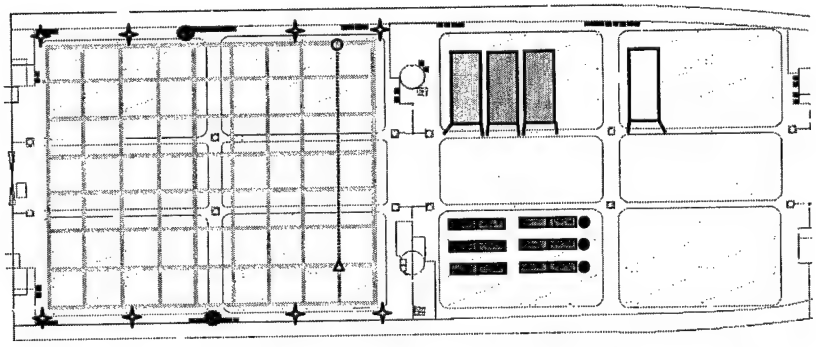

Figure A-10. Test 3 Configuration – 60-foot distance, to a corner.

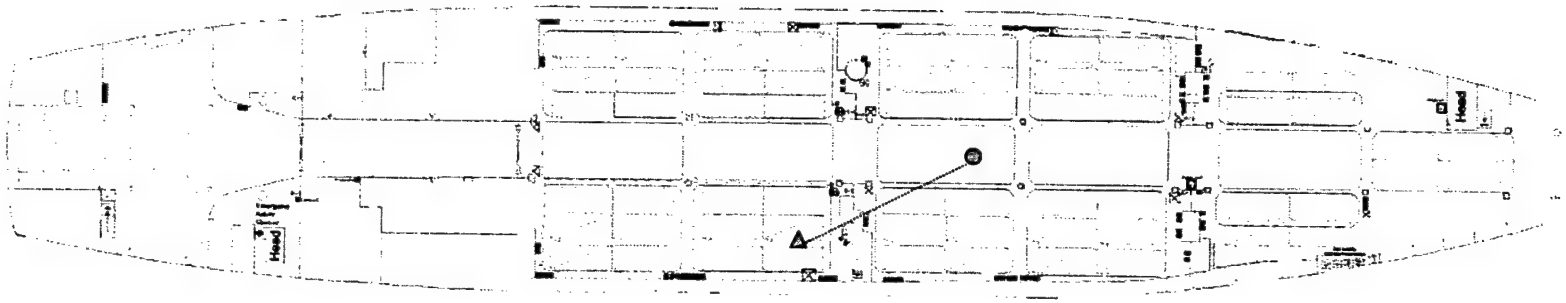

Figure A-11. Test 4 Configuration – 60-foot distance between two compartments and blocked by a bulkhead.

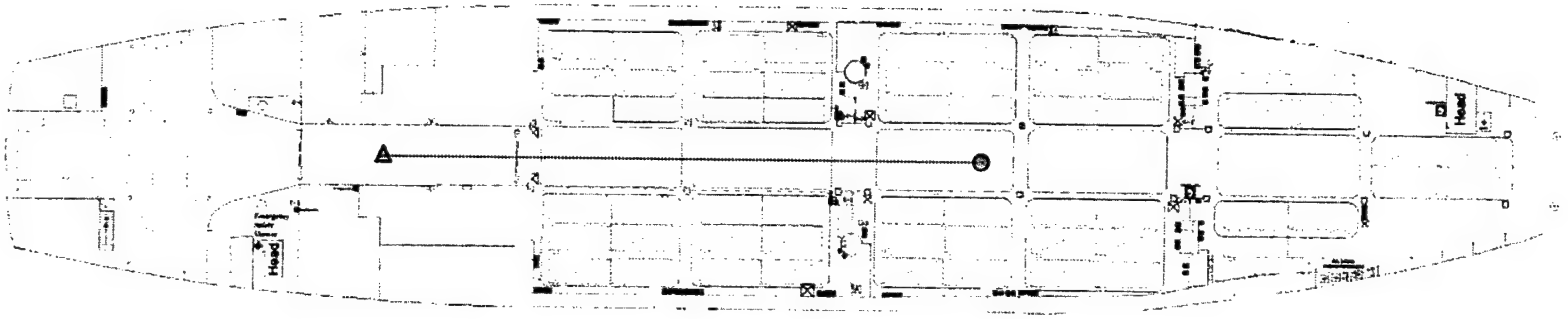

Figure A-12. Test 5 Configuration, 200-foot distance between two compartments and tunnel in direct line of sight.

Figures A-13 through A-17 show the sampling scope test results. Test 1 included 4 μsec of data. Data did not start at 0 μsec and decay times must be adjusted to account for the time offset. The high noise floor of the sampling oscilloscope of – 6 dB masked the final decay to –20 dB, the normal delay spread figure. The – 6 dB point was reached at about 1 μsec. The balance of tests included only 2 μsec of data, reducing time to take measurements. Decay time to – 20 dB is estimated to be 3 μsec.

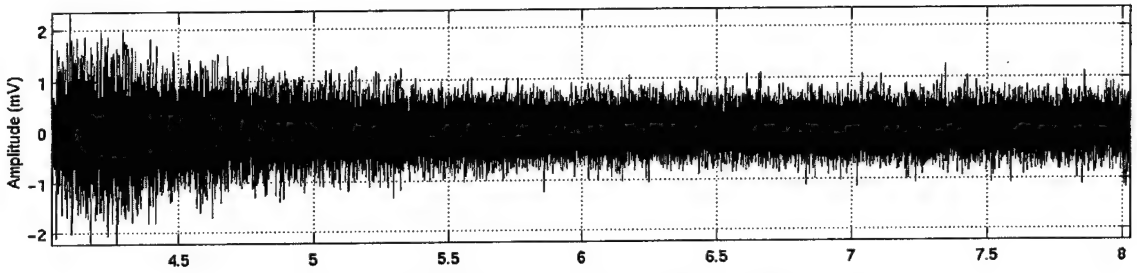

Figure A-13. Test 1 decay, sampling oscilloscope.

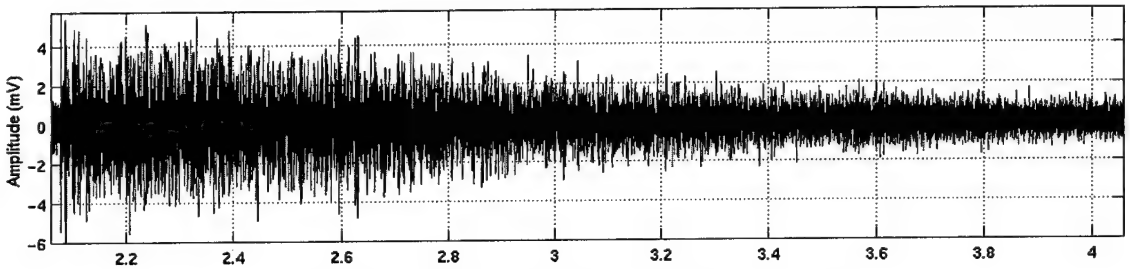

Figure A-14. Test 2 decay, sampling oscilloscope.

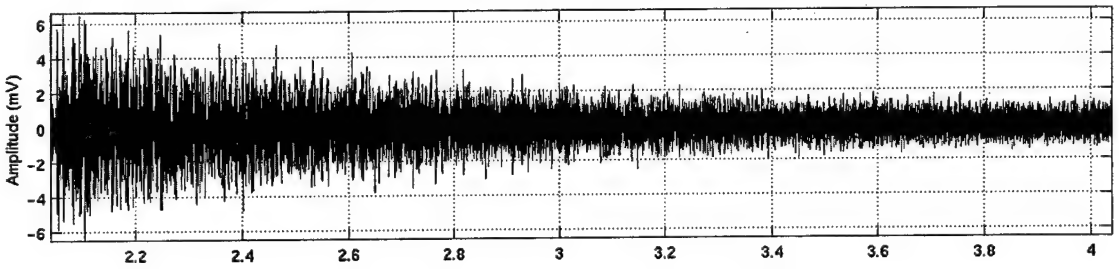

Figure A-15. Test 3 decay, sampling oscilloscope.

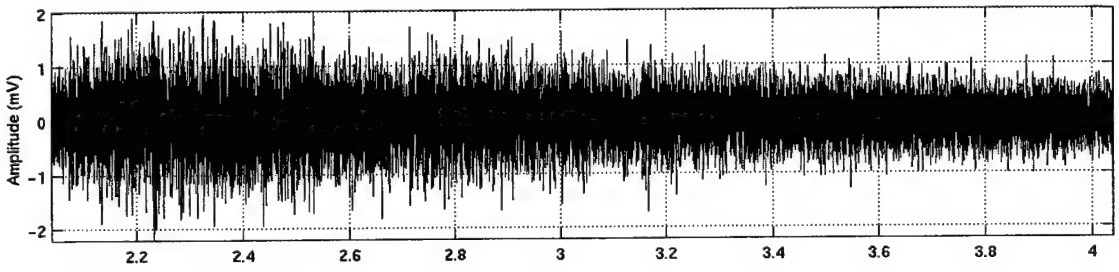

Figure A-16. Test 4 decay, sampling oscilloscope.

Test 4 shows no initial pulse, it was blocked by the bulkhead, and a slow ramp up of reverberation. Reverberation may have coupled between the two compartments through the opening, producing a double integration of energy.

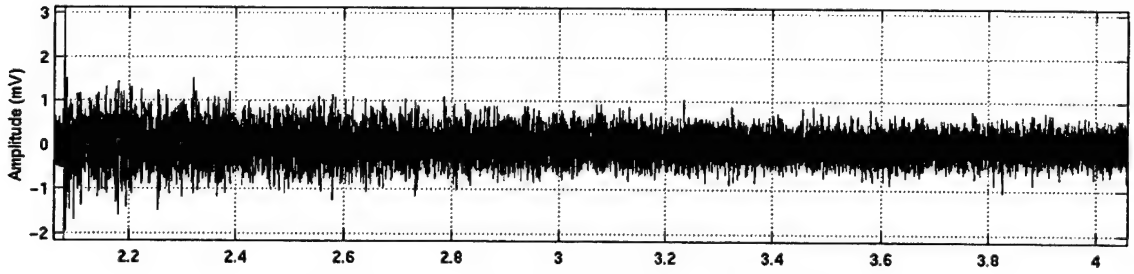

Figure A-17. Test 5 decay, sampling oscilloscope.

Test 5 shows the initial direct impulse is much higher than the overall reverberation. This may be caused by the direct line of sight filtering caused by the tunnel, providing little energy to the intervening compartment for reverberation.

Figures A-18 through A-21 shows the network analyzer measurements and Inverse Fast Fourier Transform (IFFT) for Tests 3 and 5. The network analyzer took 3,200 measurements at 1 MHz steps.

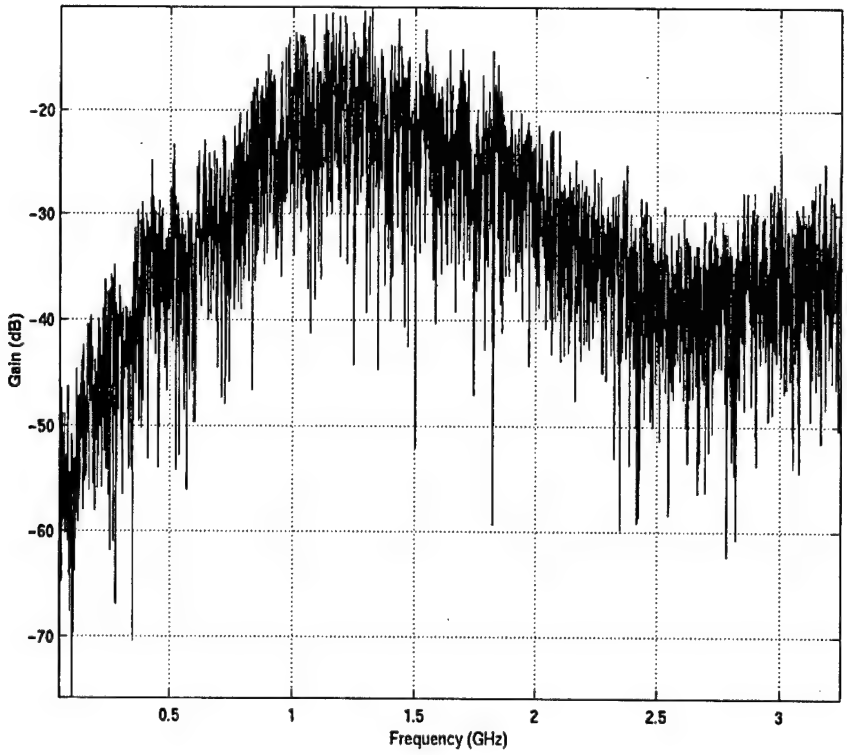

Figure A-18. Test 3 amplitude measurement, network analyzer.

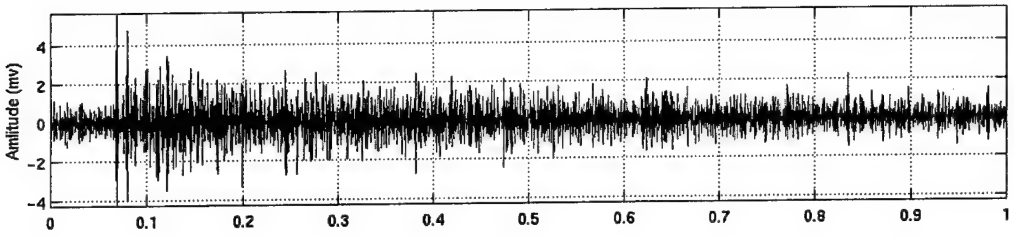

Figure A-19. Test 3 IFFT time response, network analyzer.

Figure A-18, Test 3 amplitude, the magnitude of the envelope of amplitude measurement is largely the square of the antenna responses. -6 dB responses correspond to each antenna's –3dB response. Multipath nulls are visible in the amplitude plot, extending up to 30 to 40 dB below average.

Figure A-19, Test 3 IFFT, shows the initial impulse delayed by 60 nsec, corresponding to 60-foot antenna separation. This provides excellent confirmation of the network analyzer/IFFT measurement technique.

Figure A-20, Test 5 amplitude, multipath nulls are visible in the amplitude plot, extending up to 30 to 40 dB below average.

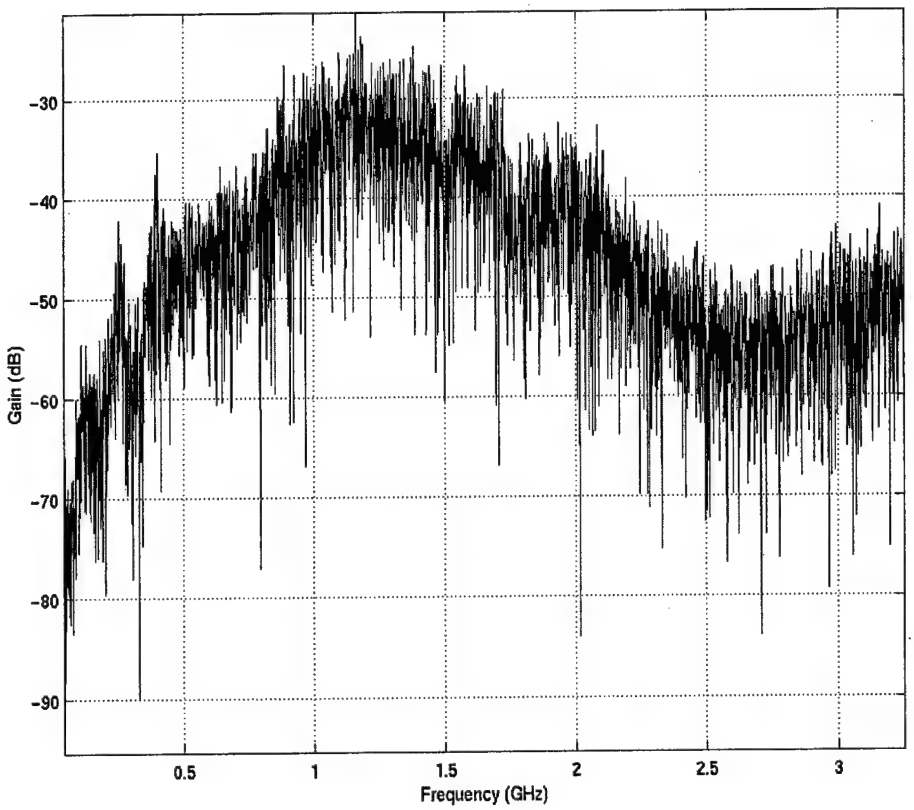

Figure A-20. Test 5 amplitude measurement, network analyzer.

Figure A-21, Test 5 IFFT, shows the initial impulse delayed by 210 nsec, corresponding to the 200-foot antenna separation. This again provides excellent confirmation of the network analyzer/IFFT measurement technique.

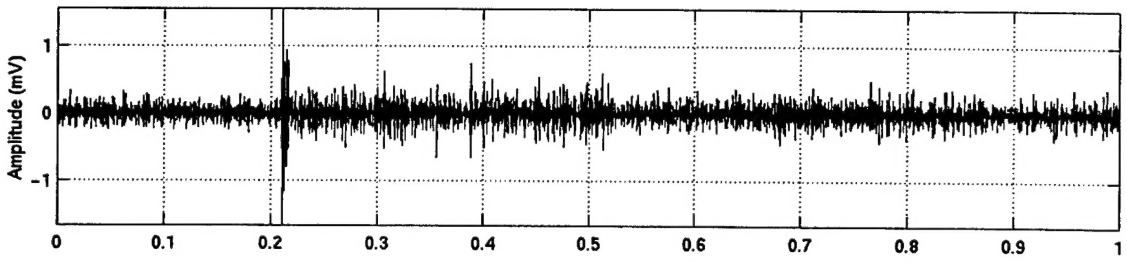

Figure A-21. Test 3 IFFT time response, network analyzer.

Figure A-22 shows a spectral measurement of a shipboard 10 GHz X-band search radar signal through a UWB antenna, made in the enclosed cargo bay of the USS Curtiss. The spectrum analyzer resolution bandwidth was 300 kHz, with *max hold* feature ON. Instantaneous or average measurements did not show significant energy. Peak measurements were required for the radar. Ship's radar emissions leaked into the closed cargo holds.

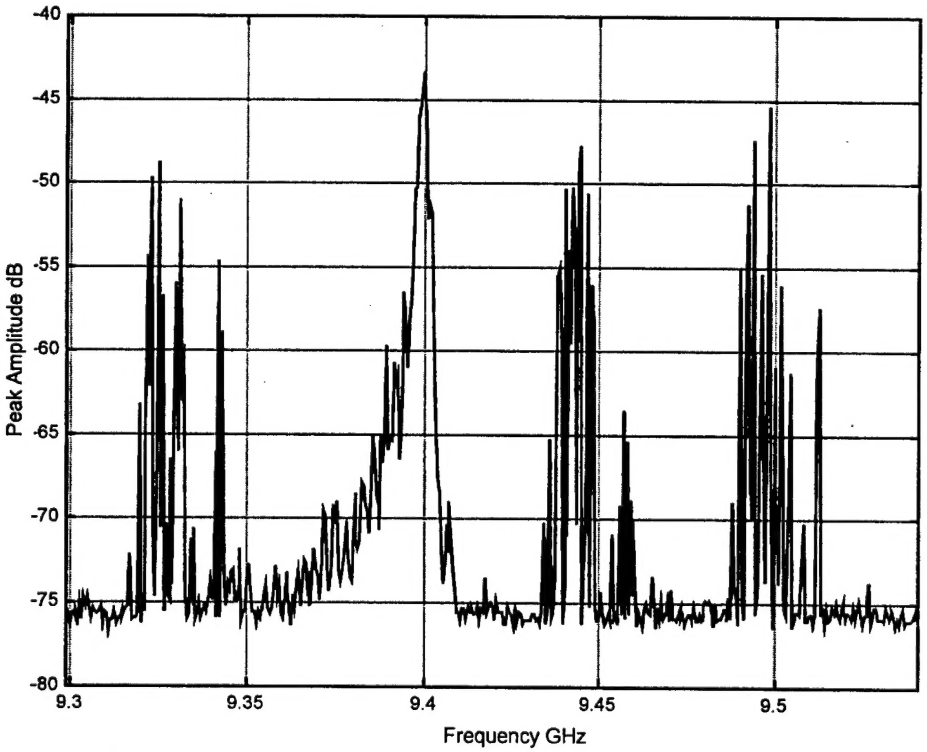

Figure A-22. Radar interference measurement, spectrum analyzer.

The scope data was auto-correlated to look for internal structure, indicating possible resonances. Figure A-23 shows a sample of oscilloscope sampled data and Figures A-24 thru A-26 show the auto-correlation. The auto-correlation showed the antenna impulse responses and no resonances. The passband of the test setup was likely too high to excite the ship's compartment cavity resonances.

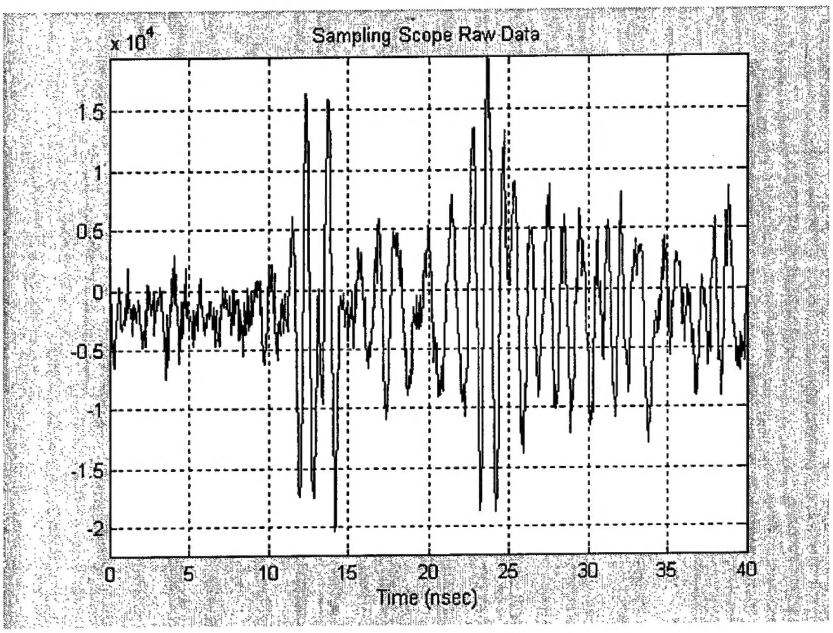

Figure A-23. Sampling scope raw data.

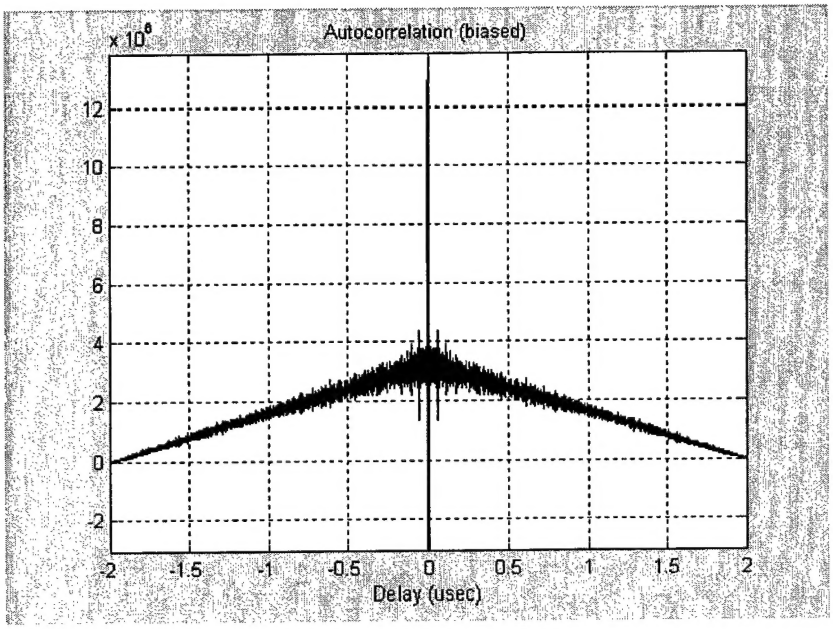

Figure A-24. Self-auto-correlation, ±2 μsec.

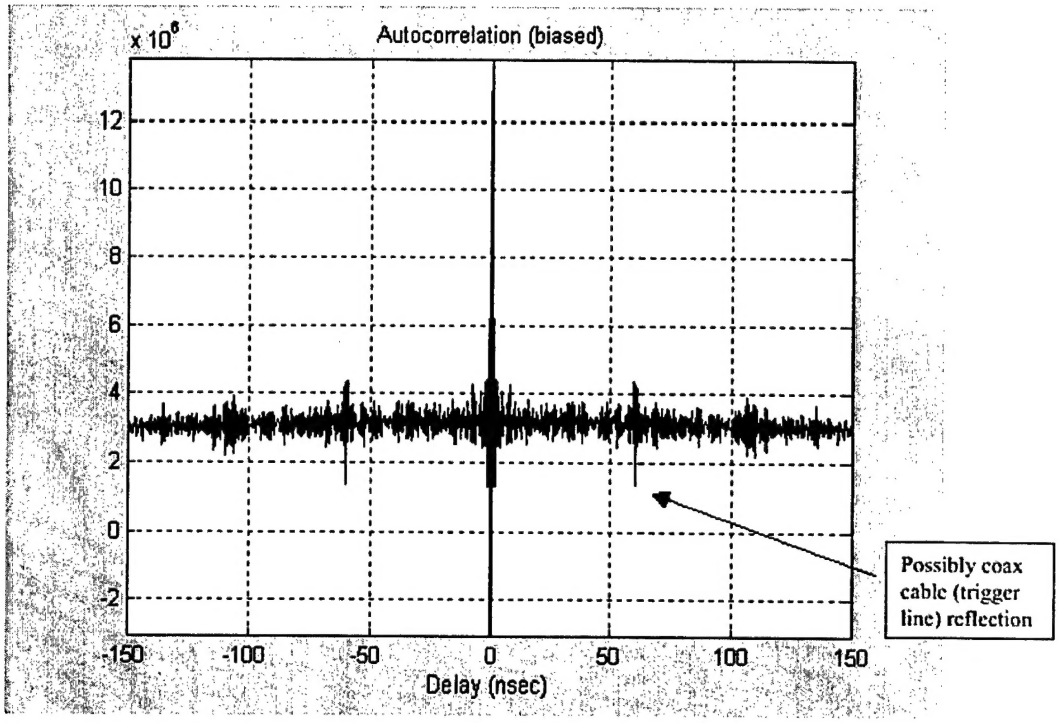

Figure A-25. Self-auto-correlation, ±50 nsec.

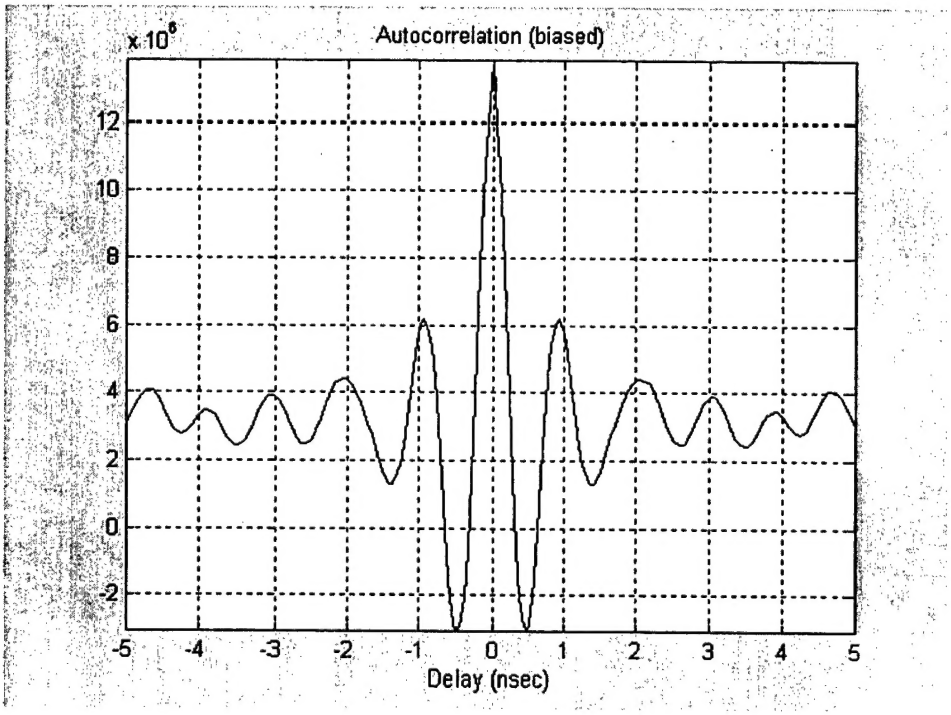

Figure A-26. Self-auto-correlation, ±5 nsec.

CONCLUSION

The SS Curtiss had very long delay spreads, approximately 1 μsec to – 6 dB, and estimated 3 μsec at –20 dB. This is approximately 10 times longer than 200 to 300 nsec typical for office and industrial environments. It is also longer than 1 μsec typical for ISO containers. The WhereNet DSSS system was designed to operate up to 1 μsec delay spread. The ship exceeded that.

Multipath nulls were measured between 30 to 40 dB using a network analyzer. They would greatly affect narrow-band systems. The multipath nulls had little effect on the DSSS system with 60-MHz spread, and the UWB system with 400-MHz instantaneous bandwidth.

The ship's 10 GHz X-band radar leaked into the compartments, but was higher in frequency than the test systems. Ship navigational radars also operated at 3.1 GHz, close but still above the 2.45 GHz ISM II frequency band used by the DSSS WhereNet system. 3.1 GHz is the lower frequency bound for full level FCC Part 15B unlicensed UWB 'C' band operation.

Ships present a challenging RF environment with deep multipath nulls and long delay spreads. Its amazing that either of the tested PAL systems worked at all.

Figures A-27 and A-28 show the USC team.

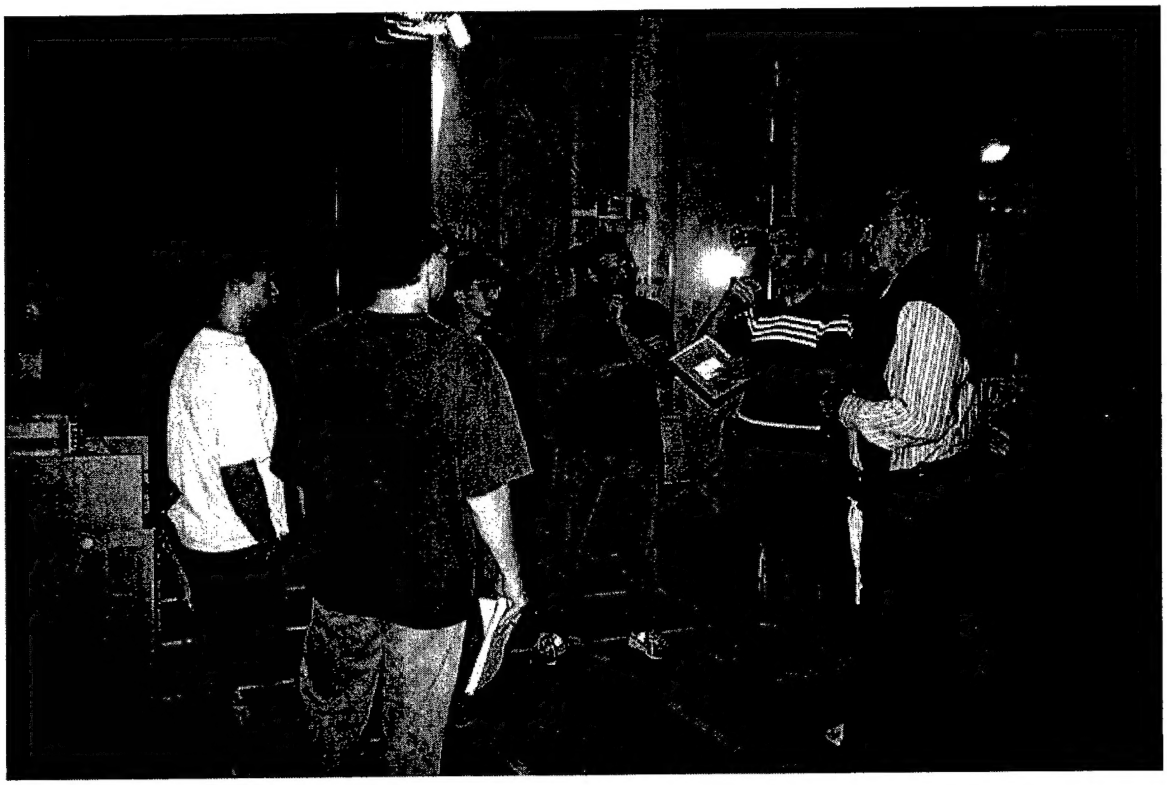

Figure A-27. USC team.